

**CONVERSION OF PALM FATTY ACID DISTILLATE TO BIOJET FUEL
OVER Ni/HY-Pd/TiO₂ CORE-SHELL CATALYST**

Chanakran Homla-or

A Thesis Submitted in Partial Fulfillment of the Requirements
for the Degree of Master of Science
The Petroleum and Petrochemical College, Chulalongkorn University
in Academic Partnership with
The University of Michigan, The University of Oklahoma,
Case Western Reserve University, and Institut Français du Pétrole
2017

บทคัดย่อและแฟ้มข้อมูลฉบับเต็มของวิทยานิพนธ์ตั้งแต่ปีการศึกษา 2554 ที่ให้บริการในคลังปัญญาจุฬาฯ (CUIR)
เป็นแฟ้มข้อมูลของนิสิตเจ้าของวิทยานิพนธ์ที่ส่งผ่านทางบัณฑิตวิทยาลัย

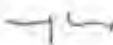
The abstract and full text of theses from the academic year 2011 in Chulalongkorn University Intellectual Repository (CUIR)
are the thesis authors' files submitted through the Graduate School.

Thesis Title: Conversion of Palm Fatty Acid Distillate to Biojet Fuel over Ni/HY-Pd/TiO₂ Core-shell Catalyst
By: Chanakran Homla-or
Program: Petroleum Technology
Thesis Advisor: Assoc. Prof. Siriporn Jongpatiwut


Accepted by The Petroleum and Petrochemical College, Chulalongkorn University, in partial fulfillment of the requirements for the Degree of Master of Science.

..... College Dean
(Prof. Suwabun Chirachanchai)

Thesis Committee:


.....
(Assoc. Prof. Siriporn Jongpatiwut)


.....
(Prof. Thirasak Rirksomboon)


.....
(Assoc. Prof. Tawan Sooknoi)

ABSTRACT

5873002063: Petroleum Technology Program

Chanakran Homla-or: Conversion of Palm Fatty Acid Distillate to Biojet Fuel over Ni/HY-Pd/TiO₂ Core-shell Catalyst.

Thesis Advisor: Assoc. Prof. Siriporn Jongpatiwut 86 pp.

Keywords: Deoxygenation/ Hydrocracking/ Hydroisomerization/ Biojet fuel/ PFAD

Generally, jet fuel is obtained from the refining of petroleum feedstock in order to power the aircrafts, hence the world is more confronting a problem with increasing air pollution emission. Therefore, biojet fuel is introduced as an alternative way to solve the problem. Biojet fuel can be derived from bio-based feedstock such as palm fatty acid distillate or PFAD. Which is converted via the deoxygenation reaction in order to remove oxygenated compounds, carboxylic and carbonyl groups in the fatty acid molecules then followed by hydrocracking and hydroisomerization reaction. The heterogeneous catalyst is used to convert PFAD into saturated paraffins in the range of jet fuels using the design of core-shell catalyst model to do both steps of deoxygenation and hydroprocessing reaction. In terms of catalyst supports, TiO₂ is used as the support in deoxygenation process to produce long chain hydrocarbon. In addition, zeolite is considered as support for hydrocracking process because of its suitable structure and acidity properties. The active metals such as Pd and Ni are also used to develop the efficiency of jet fuel production. In this work, the conversion of PFAD to biojet fuel will be investigated in a continuous flow fixed-bed reactor. The Ni/HY^{core}-Pd/TiO₂^{shell} catalyst will be prepared. During the catalytic activity testing at 425 °C, pressure 30 bar, H₂/feed molar ratio of 10, and LHSV of 1.5 h⁻¹ exhibited highest selectivity 48% towards biojet fuel. The effect of increasing space velocity did not give higher selective biojet fuel production due to shorter residence time. The formation of hydrocarbons from fatty acid over core-shell catalyst occurs through an aldehyde and alcohol intermediates further transform to heavier hydrocarbon then subsequently hydrocracking/hydroisomerization to biojet fuel.

บทคัดย่อ

ชานากานต์ หอมละออ : การสังเคราะห์น้ำมันไบโอดีเซลจากกรดไขมันปาล์มโดยใช้ตัวเร่งปฏิกิริยาแบบโครงสร้างแบบแกน-เปลือก นิกเกิลบนซีโอไลต์ Y (Ni/HY)-พาลาเดียมบนไททาเนียมไดออกไซด์ (Pd/TiO₂) (Conversion of Palm Fatty Acid Distillate to Biojet Fuel over Ni/HY-Pd/TiO₂ Core-shell Catalyst) อ. ที่ปรึกษา: รศ. ดร. ศิริพร จงผาดิวดี 86 หน้า

โดยทั่วไปน้ำมันเจ็ทสามารถผลิตได้จากกระบวนการกลั่นน้ำมันจากแหล่งเชื้อเพลิงฟอสซิล โดยการใช้ไขมันชนิดนี้จะปล่อยมลภาวะสู่ชั้นบรรยากาศในปริมาณมากซึ่งก่อให้เกิดปัญหาภาวะโลกร้อน ดังนั้นการผลิตน้ำมันไบโอดีเซลจึงจัดเป็นอีกทางเลือกหนึ่งที่ถูกนำไปประยุกต์ใช้ในอากาศยาน เนื่องจากจัดเป็นพลังงานสะอาด ที่สามารถช่วยลดมลภาวะพิษต่อธรรมชาติ ในงานวิจัยนี้จึงมุ่งเน้นในการพัฒนากระบวนการผลิตน้ำมันไบโอดีเซลจากกรดไขมันปาล์ม ซึ่งโดยปกติกรดไขมันปาล์มนั้นเป็นผลพลอยได้ที่ได้จากการกลั่นน้ำมันปาล์ม การเลือกนำกรดไขมันปาล์มมาใช้เป็นวัตถุดิบนั้นจึงได้พิจารณาจากความสนใจที่จะพัฒนาในสิ่งที่มีราคาถูกแล้วนำไปต่อยอดได้ให้ได้ประโยชน์สูงสุด น้ำมันไบโอดีเซลสามารถผลิตได้โดยผ่านกระบวนการไฮโดรต็อกซิฟิเคชัน, ดีคาร์บอนิเลชัน/ ดีคาร์บอกซิเลชัน เพื่อขจัดสารประกอบออกซิเจน, หมู่คาร์บอนิล และหมู่คาร์บอกซิล ออกจากกรดไขมันปาล์ม ตามด้วยกระบวนการไฮโดรแครกกิง เพื่อให้โมเลกุลของสายโซ่แตกตัวเล็กลง โดยใช้ตัวเร่งปฏิกิริยาแบบวิวิธพันธ์ ทำงานในเตาปฏิกรณ์ระบบเบดคงที่ภายใต้แก๊สไฮโดรเจนและความดันสูง เพื่อเร่งให้เกิดปฏิกิริยาทางเคมี โดยตัวเร่งปฏิกิริยาที่ใช้นั้นคือตัวเร่งปฏิกิริยาที่มีโครงสร้างแบบแกน-เปลือก โดยในส่วนแกนนั้นคือนิกเกิลบนซีโอไลต์ Y (Ni/HY) และในส่วนเปลือกนั้นคือพาลาเดียมบนไททาเนียมไดออกไซด์ (Pd/TiO₂) ตัวเร่งปฏิกิริยาส่วนแกนจะเตรียมโดยการเติมโลหะ Ni ลงไปบนตัวรองรับซีโอไลต์ Y ด้วยวิธีการเคลือบฝังด้วยเทคนิคแบบเปียกพอดี้กับพื้นผิว (incipient wetness impregnation) ที่ร้อยละ 5, 10 และ 15 เปอร์เซ็นต์โดยน้ำหนัก หลังจากนั้นการสังเคราะห์ส่วนเปลือกเคลือบส่วนแกน Pd/TiO₂ ด้วยเทคนิควิธีโซลเจลขั้นตอนเดียว (single step sol gel) เนื่องจากจะให้พื้นที่ผิวสูงสุดเพื่อให้เกิดการกระจายตัวของโลหะ Pd ที่ดี โดย หลังจากนั้นนำตัวเร่งที่ได้ไปเผาที่อุณหภูมิ 500 องศาเซลเซียส เพื่อเปลี่ยนโลหะในสารละลายที่ใช้ให้อยู่ในรูปโลหะออกไซด์ แล้วนำตัวเร่งปฏิกิริยาที่ได้ไปทดสอบประสิทธิภาพ โดยพบว่าที่อุณหภูมิ 425 องศาเซลเซียส และค่า LHSV (Liquid Hourly Space Velocity) ที่ 1.5 ต่อชั่วโมง สามารถผลิตน้ำมันไบโอดีเซลได้ถึง 48%

ACKNOWLEDGEMENTS

First of all, I am deeply grateful to my advisor, Assoc. Prof. Siriporn Jongpatiwut, for the supervisions, inspiration, suggestions, and encouragements throughout this research. This special project would not have been completely finished without their precious advised and supports.

I would like to express my sincere thanks to Prof. Thirasak Rirksomboon and Assoc. Prof. Tawan Sooknoi for kindly serving on my thesis committee. Their suggestions are certainly important and helpful for completion of this thesis.

I would like to acknowledge the financial support from Center of Excellence on Petrochemical and Materials Technology and PTT Public Company Limited for partial research expense.

Moreover, I would like to thank all faculty and staff at The Petroleum and Petrochemical College, Chulalongkorn University for their kind assistance and cooperation.

I would like to thank Mr. Katipot Inkong for all of his assistance, Ms. Wipada Yenying, Ms. Yanika Sangasang, and all of my seniors at KMITL for their suggestions and my PPC friends for all support and encouragement.

I also would like to thank Mr. Yodsathorn Chavewanmas for his support during my work time of research and Mr. Surachet Soontontaweesub for his moral support and listening at all of my problems, he also encourage me in hard time since every step I had been here.

Finally, I would like to express my sincere gratitude to thank my family, for showing me the joy of intellectual pursuit ever since I was a child, for standing by me and for understanding every single part of my mind.

TABLE OF CONTENTS

	PAGE
Title Page	i
Abstract (in English)	iii
Abstract (in Thai)	iv
Acknowledgements	v
Table of Contents	vi
List of Tables	ix
List of Figures	xi
 CHAPTER	
I INTRODUCTION	1
 II LITERATURE REVIEW	
2.1 Biojet Fuel	3
2.2 Bio-hydrogenated Fuel Feed Stock	4
2.3 Palm Fatty Acid Distillate Feedstock	6
2.4 The Overall Reaction For Biojet Fuel Production	10
2.4.1 Hydrodeoxygenation	10
2.4.2 Hydrocracking	12
2.4.3 Hydroisomerization	15
2.4.4 Hydrogenation and Dehydrogenation	18
2.4.5 Hydrogenolysis	19
2.5 Catalyst For Biojet Production	19
2.5.1 Core-shell Catalyst	20
2.5.2 Zeolite	22
2.5.3 Titanium Dioxide	27
2.5.4 Metal Catalyst	29

CHAPTER		PAGE
III	EXPERIMENTAL	31
	3.1 Materials and Equipment	31
	3.1.1 Materials	31
	3.1.2 Equipment	32
	3.2 Experimental Procedures	33
	3.2.1 Preparation of 5wt.% Ni Supported HY Catalyst	33
	3.2.2 Core-shell Catalyst Preparation	33
	3.3 Catalyst Characterization	34
	3.3.1 X-ray Diffractometer (XRD)	34
	3.3.2 X-ray Photoelectron Spectroscopy (XPS)	34
	3.3.3 Brunauer-Emmett-Teller (BET)	34
	3.3.4 Temperature Programmed Reduction (TPR)	34
	3.3.5 Temperature Programmed Desorption (TPD) of Isopropylamine	35
	3.3.6 Temperature Programmed Oxidation (TPO)	35
	3.3.7 Transmission Electron Microscopy (TEM)	36
	3.3.8 Gas Chromatography with Time-of-Flight Mass Spectrometer (GC-TOFMS)	36
	3.4 Catalyst Activity Testing	37
	3.5 Product Analysis	39
	3.5.1 Liquid Products Analysis	39
	3.5.2 Gas Products Analysis	40
IV	RESULTS AND DISCUSSION	42
	4.1 Characterization of Fresh Catalysts	42
	4.1.1 Xray Diffraction (XRD)	
	4.1.2 X-ray Photoelectron Spectroscopy (XPS)	43
	4.1.3 Transmission Electron Microscope (TEM)	45
	4.1.4 Brunauer-Emmett-Teller (BET)	46

CHAPTER	PAGE
4.1.5 Temperature Programmed Desorption (TPD) of Isopropylamine	47
4.1.6 Temperature Programmed Reduction (TPR)	48
4.2 Gas Chromatography of Feed and Standard Analysis	49
4.2.1 Feed Analysis	49
4.2.2 Standard Analysis	50
4.3 Catalytic Activity Testing	54
4.3.1 Effect of Core-shell Catalyst	54
4.3.2 Effect of Reaction Temperature	60
4.3.3 Effect of Reaction Pressure	62
4.3.4 Effect of LHSV	63
4.4 Reaction Pathway	64
4.5 Characterization of Spent Catalysts	71
4.5.1 Temperature-Programmed Oxidation (TPO)	71
V CONCLUSIONS AND RECOMMENDATIONS	73
REFERENCES	75
APPENDIX	78
Appendix A1 Overall Mass Balance of Deoxygenation- hydroprocessing at Different in Temperature	78
Appendix A2 Overall Mass Balance of Deoxygenation- hydroprocessing at Different in Pressure	80
Appendix A3 Overall Mass Balance of Deoxygenation- hydroprocessing at Different in Liquid Hourly Space Velocity	82

CHAPTER	PAGE
Appendix A4 Overall Mass Balance of Deoxygenation- hydroprocessing One-pot Reaction over Pd/TiO ₂ , Ni/HY, and 5%Ni/HY ^{core} -1%Pd/TiO ₂ ^{shell} Catalysts	84
CURRICULUM VITAE	86

LIST OF TABLES

TABLE	PAGE
2.1 A variety of feedstocks for production of biodiesel	5
2.2 The chemical structure of common fatty acids in vegetable oils	6
2.3 The properties of fatty acid distillates from palm oil	8
2.4 Summary of catalyst sample parameters, activity, and selectivity for onepot oxidation	22
2.5 Zeolites classified by window size	24
3.1 Description of system in flow diagram of the continuous flow fixed-bed reactor	38
3.2 The reaction conditions for hydroprocessing of palm fatty acid distillate in continuous flow fixed-bed reactor	39
3.3 The chromatographic temperature program for liquid product analysis	40
3.4 The chromatographic temperature program for gas-phase product analysis	41
4.1 Physical characteristics of the prepared catalysts.	47
4.2 Acidity of the prepared catalysts from TPD of isopropylamine	48
4.3 Composition of PFAD feedstock	50
4.4 Amount of carbon deposits on prepared catalyst after reaction	72
A1 Overall mass balance of deoxygenation-hydroprocessing one-pot reaction over 5%Ni/HY ^{core} -1%Pd/TiO ₂ ^{shell} catalyst at different in temperature. (Reaction condition: 5 bar, H ₂ /feed molar ratio of 10, LHSV of 1.5 h ⁻¹ , and TOS at 6h)	76

TABLE		PAGE
A2	Overall mass balance of deoxygenation-hydroprocessing one-pot reaction over 5%Ni/HY ^{core} -1%Pd/TiO ₂ ^{shell} catalyst at different in pressure. TOS at 6h)	78
A3	Overall mass balance of deoxygenation-hydroprocessing one-pot reaction over 5%Ni/HY ^{core} -1%Pd/TiO ₂ ^{shell} catalyst at different in LHSV. (Reaction condition: 425 °C, pressure 30 bar, H ₂ /feed molar ratio of 10, and TOS at 6h)	80
A4	Overall mass balance of deoxygenation-hydroprocessing one-pot reaction over Pd/TiO ₂ , Ni/HY, and 5%Ni/HY ^{core} -1%Pd/TiO ₂ ^{shell} catalysts. (Reaction condition: 425 °C, pressure 30 bar, H ₂ /feed molar ratio of 10, LHSV of 1.5 h ⁻¹ and TOS at 6h)	82

LIST OF FIGURES

FIGURE	PAGE
2.1	World palm oil productions in 2009. 7
2.2	The production yield of oil from various sources biodiesel feedstock. 7
2.3	Main reactions occur in deoxygenation of triglycerides. 11
2.4	The schematic of hydro cracking reaction. 12
2.5	Typical reaction path way in hydrocracking of <i>n</i> -paraffins. 13
2.6	Effect of reaction temperature on iso-to-normal paraffin ratio in products obtained from hydrocracking of <i>n</i> -decane over strongly acidic catalyst. 14
2.7	The distribution of carbon number in catalytic cracking and hydrocracking of <i>n</i> -hexadecane during 50% conversion. 14
2.8	The bi-functional pathways of hydroisomerization and cracking of <i>n</i> -paraffins. 17
2.9	Schematic of hydrogenolysis reaction. 19
2.10	(a) Kinetics of methyl phenyl sulfide one-pot oxidation and (b) dependence of the conversion level on the selectivity using Pd/SiO ₂ @Ti-MS or SiO ₂ @Pd(S)/Ti-MS type core-shell catalysts with various shell thicknesses (different amounts of precursors; 1, 3, 5, and 7 times the original amount). 21
2.11	Formation of three common zeolites from primary units. 23
2.12	Three commercial zeolites of difference dimensionalities. 24
2.13	The 3D illustrate of Y zeolite structure. The silicon or aluminum ions are located at the corners and the oxygen ions near the edges. 26
3.1	The schematic diagram of the reactor system. 37

FIGURE	PAGE
4.1 XRD patterns of synthesized parent HY, Ni/HY, Ni/HYcore-Pd/ TiO ₂ ^{shell} , and Pd/TiO ₂ catalysts.	43
4.2 High resolution XPS spectrum of Pd 3d in Pd/TiO ₂ .	44
4.3 High resolution XPS spectrum of Ni 2p in Ni/HY.	44
4.4 (a), (b) TEM images of Ni/HY catalyst.	45
4.5 (a), (b) TEM images of Pd/TiO ₂ ^{shell} catalyst.	46
4.6 (a), (b) TEM images TEM images Ni/HY ^{core} -Pd/TiO ₂ ^{shell} catalyst.	46
4.7 TPD profiles of prepared catalysts.	48
4.8 Temperature programmed reduction (TPR) profiles of the prepared Ni/HY and Ni/HY ^{core} -Pd/TiO ₂ ^{shell} catalysts.	49
4.9 The chromatogram of various fatty acids components in PFAD range analyzed by a GC/FID.	50
4.10 Chromatograms of standard oxygenated compounds.	51
4.11 Chromatograms of standard <i>n</i> -alkanes.	51
4.12 (a) Feed palm fatty acid distillate, (b) Liquid products, (c) liquid products chromatogram, and (d) gas products chromatogram over Ni/HY ^{core} -Pd/TiO ₂ ^{shell} catalyst operated at operating conditions: 425 °C, 30 bar, LHSV of 1.5 h ⁻¹ , H ₂ /feed molar ratio of 10, and TOS of 6 h.	52
4.13 The conversion and selectivity of products that obtained over 1%Pd/TiO ₂ shell, 5%Ni/HY core, and 5%Ni/HY ^{core} -1%Pd/TiO ₂ ^{shell} (Reaction condition: reaction temperature 425 °C, 30 bar, H ₂ /feed molar ratio of 10, LHSV of 1.5 h ⁻¹ , and TOS at 6h).	55

FIGURE	PAGE
4.14 The conversion and selectivity of products that obtained over 1%Pd/TiO ₂ (shell) at reaction condition: 425 °C, 30 bar, LHSV of 1.5 h ⁻¹ , and H ₂ /feed molar ratio of 10.	56
4.15 Product distribution of bio-jet production from PFAD over 1%Pd/TiO ₂ (shell) catalyst at operating condition: 425 °C, 30 bar, LHSV of 1.5 h ⁻¹ , H ₂ /feed molar ratio of 10 and TOS of 6 h.	57
4.16 The conversion and selectivity of products that obtained over 5% Ni/HY (core) at reaction condition: 425 °C, 30 bar, LHSV of 1.5 h ⁻¹ , and H ₂ /feed molar ratio of 10.	58
4.17 Product distribution of bio-jet production from PFAD over 5%Ni/HY (core) catalyst at operating condition: 425 °C, 30 bar, LHSV of 1.5 h ⁻¹ , H ₂ /feed molar ratio of 10 and TOS of 6 h.	58
4.18 The conversion and selectivity of products that obtained over 5%Ni/HY ^{core} -1%Pd/TiO ₂ ^{shell} at reaction condition: 425 °C, 30 bar, LHSV of 1.5 h ⁻¹ , and H ₂ /feed molar ratio of 10.	59
4.19 Product distribution of bio-jet production from PFAD over 5%Ni/HY ^{core} -1%Pd/TiO ₂ ^{shell} catalyst at operating condition: 425 °C, 30 bar, LHSV of 1.5 h ⁻¹ , H ₂ /feed molar ratio of 10, and TOS of 6 h.	60
4.20 The conversion and selectivity of products that obtained over 5%Ni/HY ^{core} -1%Pd/TiO ₂ ^{shell} at different temperature (Reaction condition: 5 bar, H ₂ /feed molar ratio of 10, LHSV of 1.5 h ⁻¹ , and TOS at 6h).	61

FIGURE	PAGE
4.21 The product distribution over 5%Ni/HY ^{core} -1%Pd/TiO ₂ ^{shell} at different temperature (Reaction condition: 5 bar, H ₂ /feed molar ratio of 10, LHSV of 1.5 h ⁻¹ , and TOS at 6h).	61
4.22 The conversion and selectivity of products that obtained over 5%Ni/HY ^{core} -1%Pd/TiO ₂ ^{shell} at different pressure (Reaction condition: reaction temperature at 425 °C, H ₂ /feed molar ratio of 10, LHSV of 1.5 h ⁻¹ , and TOS at 6h).	62
4.23 The conversion and selectivity of products that obtained over 5%Ni/HY ^{core} -1%Pd/TiO ₂ ^{shell} at different LHSV (Reaction condition: reaction temperature at 425 °C, 5 bar, H ₂ /feed molar ratio of 10, and TOS at 6h).	63
4.24 Proposed reaction pathway of biojet production from PFAD over Pd/TiO ₂ .	65
4.25 Selectivity of intermediates from biojet fuel production over Pd/TiO ₂ at reaction condition: 425 °C, 30 bar, LHSV of 1.5 h ⁻¹ , and H ₂ /feed molar ratio of 10.	65
4.26 The mass spectrum of wax that obtained from GC/MS of 1-hexadecanol from NIST Library.	66
4.27 Proposed reaction pathway of biojet production from PFAD over Ni/HY.	66
4.28 Selectivity of intermediates from biojet fuel production over Ni/HY at reaction condition: 425 °C, 30 bar, LHSV of 1.5 h ⁻¹ , and H ₂ /feed molar ratio of 10.	67
4.29 Proposed reaction pathways of deoxygenation of fatty acid.	67
4.30 Selectivity of intermediates from biojet fuel production over 5%Ni/HY ^{core} -1%Pd/TiO ₂ ^{shell} at reaction condition: 425 °C, 30 bar, LHSV of 1.5 h ⁻¹ , and H ₂ /feed molar ratio of 10.	68
4.31 Proposed reaction pathway of palmitic acid to hydrocarbons.	69

FIGURE		PAGE
4.32	Proposed reaction pathways of oleic acid to hydrocarbons.	70
4.33	TPO profiles of Ni/HY ^{core} -Pd/TiO ₂ ^{shell} , Ni/HY, and Pd/TiO ₂ catalysts after 8 h course of reaction.	71

CHAPTER I

INTRODUCTION

Over the last few years, the transportation by aircraft was increasing so it led to more jet fuel consumption of the world. Generally, jet fuel, also known as aviation fuel, is obtained from the refining of petroleum feedstock in order to powering the aircrafts, which contain only hydrocarbon resulting in high heat combustion and compatibility with turbine engines. Due to conventional jet fuel obtaining from fossil fuel resources, hence the world is more confronting a problem with increasing air pollution emission. Therefore, many researchers try to develop alternative energy like biojet fuel from bio-based feedstock to solve the problem because biojet fuel is a green energy, renewable energy, and environmental friendly product.

Accordingly, the numerous vegetable oils for instance palm, soybean, rapeseed, and jatropha are normally used to produce biofuel in order to replace petroleum fuel because it is renewable resources, contains low aromatics and sulfur, and can reduce environmental pollution. Recently, palm is well-known in several countries as alternative resources used in crude palm oil refinery. Throughout the refining of crude palm oil, lower value fatty acids residue is generated by stripping column then condensed into fatty acid distillate product which known as palm fatty acid distillate or PFAD. PFAD is normally used in soap industries, oleochemical industries, and biofuel production. Because of the cheaper price of PFAD comparing with palm oil feedstock, thus the way to provide valuable products such as biojet fuel from PFAD become more interesting.

Biojet fuels can be produced via hydrodeoxygenation, hydrodecarboxylation/ hydrodecarbonylation in order to remove oxygenated compounds, carboxylic and carbonyl groups in the fatty acid molecules then followed by hydroprocessing which involves hydrogenation, hydrocracking and hydroisomerization reaction. The heterogeneous catalyst is used to convert PFAD into saturated paraffins in the range of jet fuels. There are several active metals used in these reactions such as Pd, Pt, Ni, Mo, Co, etc. In addition, zeolite is considered as support because of its suitable structure and acidity properties. However, the reaction

condition is favorable at high hydrogen partial pressure to become excess hydrogen consumption because excess hydrogen will lead to the lower olefins formation and higher desired paraffins product.

Accordingly, the development of core-shell catalyst model should be considered in terms of conversion, selectivity, stability, and economics. In term of catalyst supports, TiO_2 exhibited high efficiency in deoxygenation process to produce long chain hydrocarbon. In addition, HY zeolite is considered as support for hydrocracking process because of its suitable structure and acidity properties. The active metals such as Pd and Ni are also used to develop the efficiency of jet fuel production. Thus, Ni is one of the interesting transition metals used to develop jet fuel production because the efficiency is similar to Pt and relatively low price. In the previous studies, the catalyst was synthesized via a combined single-step sol-gel (SSSG) process. It can be revealed that the catalyst with 36% shell composition gave the highest biojet fuel yield.

In this study, the conversion of PFAD to bio-jet fuels will be investigated in a continuous flow fixed-bed reactor. The Ni/HY, Pd/ TiO_2 , and Ni/HY^{core}-Pd/ TiO_2 ^{shell} catalysts will be prepared by incipient wetness impregnation, sol-gel, and SSSG with 36% shell methods, respectively. The catalysts will be used to investigate the conversion and selectivity of during the catalytic activity testing. Moreover, the effect of pressure, space velocity and temperature are also be optimized to satisfy the yield of bio-jet fuels.

CHAPTER II

LITERATURE REVIEW

Jet fuel also generally known as aviation fuels is a type of petroleum fuel used to power the aircraft by gas turbine power unit. Jet fuel is straw-coloured liquid which is basically containing a large number of hydrocarbon mixtures. There are two standard international specification of aviation in market which are Jet A and Jet A-1. Jet A and Jet A-1 are kerosene-type (C8-C16) fuels that could be distinguish by the difference of the freezing point, the temperature at which wax crystals disappear in a laboratory test. In the United States, Jet A must have a freezing point of -40 °C or below and normally not contain an additive while Jet A-1 must have a freeze point of -47 °C or below and contains an additive for using in the state not located in US. Another type of jet fuel is Jet B is naphtha-kerosene (C5-C15) and has a very low freezing point of -60 °C which used to perform in cold weather. Jet fuel particularly derived from distillate crude oil in refinery. The production of jet fuel has to suitable for turbine engines and suitable for internal combustion engines. Jet fuel used aircraft should be low viscosity at low temperature, chemical stability in high temperature, clean combustion, and reach the specific limitation in density and calorific parameters.

Recently, the instable price of fossil fuel and environmental issue are the reasons for develop alternative sustainable energy which friendly with environment, inexpensive, meet the specification with the market.

2.1 Biojet Fuel

A biojet fuel also known as aviation biofuel used for aircraft. In a few years, the industry turned to second generation sustainable biofuels (sustainable aviation fuels) that friendly with agricultural land or fresh water.

As aviation fuel distribute of the greenhouse gas emissions, as air travel increases and increased of the number vehicles, ethanol and biodiesel as alternative fuels are more interested. In addition, to building more fuel efficient aircraft and

operating them more efficiently, the fuel resource is one of the few choice of the aviation industry has for reducing its carbon footprint.

Jatropha is one source of potential for biofuels production, estimated using it could reduce greenhouse gas emissions by up to 85% if former agro-pastoral land is used, or increase emissions by up to 60% if natural woodland is converted to use. In addition, biofuels do not contain sulfur compounds and thus do not release sulfur dioxide to the air.

2.2 Bio-hydrogenated Fuel Feedstock

Generally, vegetable oil is used for bio fuel production due to more advantages aspect of agricultural economy, stable material to provide, and environmental. There are many choice of vegetable oil to be choose depend on agriculture in local land and transportation cost in each country. Normally, vegetable oil is composed of triglyceride which is long chain carbon atoms in a range of 16–24 with oxygenated compound in its chemical structure. Table 2.1 shows various resources both edible oil; soybean oil, rapeseed oil, and palm oil etc. and non-edible oil; algae and jatropha that many research use to investigate the reaction of alternative fuel production.

Recently, those vegetable oils can be used to produce green fuel to meet the specification of sustainable energy market for future energy. Furthermore, it also decrease problem of environmental because it can reduce the effect of gases emission for instance carbon dioxide, carbon monoxide, sulfur oxide, and polycyclic aromatic hydrocarbon(PAH) (Talebian-Kiakalaieh *et al.*, 2013).

Triglycerides in vegetable oils are a combination of glycerol and fatty acids which can be separated by carbon length. There are approximate around 300 types of fatty acids derivation both vegetable oils and animal fats. The most common fatty acids in vegetable oils such as stearic, oleic, linolenic and palmitic are shown in Table 2.2..The heating values of vegetable oils are around 39–40 MJ/kg which higher than FAME (Fatty Acid Methyl Ester) required of European Union standard EN 14214 for biodiesel fuel minimum HHV (High Heating Value) at 35 MJ/kg.

Table 2.1 A variety of feedstocks for production of biodiesel (Talebian-Kiakalaieh *et al.*, 2013)

Conventional feedstock		Non-conventional feedstock
Mahua	Soybean	Lard
Nile tilapia	Rapeseed	Tallow
Palm	Canola	Poultry fat
Poultry	Babassu	Fish oil
Tobacco seed	Brassica carinata	Bacteria
Rubber plant	Brassica napus	Algae
Rice bran	Copra	Fungi
Sesame	Groundnut	Micro-algae
Sunflower	Cynara cardunculus	Tarpenes
Barley	Cottonseed	Latexes
Coconut	Pumpkin	Pongamina pinnata
Corn	Jobba oil	Palanga
Used cooking oil	Camelina	Jatropha curcas
Linseed	Peanut	Sea mango
Mustard	Olive	Okra

Jatropha (*Jatropha curcas*) is one that known of non-edible oils, it is a drought-resistant, rapidly growth, easy propagation so can be planted in variability climate conditions for example severe heat, both low rainfall and high rainfall, and frost. Recently, jatropha is represented for diesel replacement which effectively reduces CO₂ concentrations in the atmosphere when it is applied in diesel engine. Jatropha is very popular in developing countries particular India; it has been used as the major resource of biodiesel. Therefore, Jatropha become more interested in term of potential oil resource as a feedstock for biodiesel production. However, direct burning of Jatropha oil in diesel engine cause in many problems related to viscosity which is higher than diesel due to large molecular weight and chemical structure (Ong *et al.*, 2011).

Table 2.2 The chemical structure of common fatty acids in vegetable oils (Ong *et al.*, 2011)

Name	Chemical name	Structure (xx:y) ^a	Formula
Lauric	Dodecanoic	12:0	C ₁₂ H ₂₄ O ₂
Myristic	Tetradecanoic	14:0	C ₁₄ H ₂₈ O ₂
Palmitic	Hexadecanoic	16:0	C ₁₆ H ₃₂ O ₂
Stearic	Octadecanoic	18:0	C ₁₈ H ₃₆ O ₂
Oleic	cis-9-Octadecenoic	18:1	C ₁₈ H ₃₄ O ₂
Linoleic	cis-9,cis-12-Octadecadienoic	18:2	C ₁₈ H ₃₂ O ₂
Linolenic	cis-9,cis-12,cis-15-Octadecatrienoic	18:3	C ₁₈ H ₃₀ O ₂
Arachidic	Eicosanoic	20:0	C ₂₀ H ₄₀ O ₂
Gadoleic	11-eicosenoic	20:1	C ₂₀ H ₃₈ O ₂
Behenic	Docosanoic	22:0	C ₂₂ H ₄₄ O ₂
Erucle	cis-13-Docosenoic	22:1	C ₂₂ H ₄₂ O ₂
Lignoceric	Tetracosanoic	24:0	C ₂₄ H ₄₈ O ₂

a) xx = total number of carbon atoms and y = number of double bonds.

2.3 Palm Fatty Acid Distillate Feedstock

Palm is a tropical plant represented as one of edible oil which can be grows in pasture land together with humid, It is provide greater oil yield than soybean oil about 10 times approximate around 4–5 tonnes of oil per year round. In a few decades, the global demand of edible oil such as soybean and oil palm is increasing meanwhile South East Asia is the highest palm oil production in 2009 with total average around 89% especially Indonesia followed by Malaysia respectively as shown in Figure 2.1 According to palm oil is the most efficient oil in terms of land advantage, efficiency and profitability thus palm oil becomes the choice for biodiesel.

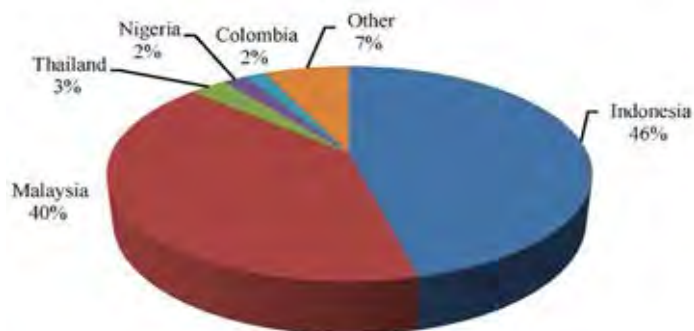


Figure 2.1 World palm oil productions in 2009.

Nowadays, above 95% of biodiesel which is produced from edible oil can be easily available to upgrade from the agricultural industry into large scale factory. Figure 2.2 displayed the production yield of oil from various sources biodiesel feedstock. Oil palm gives the highest oil productivity followed by soybean oil, calophyllum inophyllum, coconut, and jatropha. Palm oil is the leader of biodiesel production rate to meet the future specification demand due to its high oil content approximately 6000 liters of palm oil can be produced 4800 liters of biodiesel (Karmakar *et al.*, 2015). The study of Life cycle analysis (LCA) demonstrated that biodiesel based on palm oil can reduce greenhouse gases emission very effectiveness in a number of 62% as compared to soybean oil, rapeseed oil and sunflower oil which reduce by 40%, 45%, and 58% respectively.

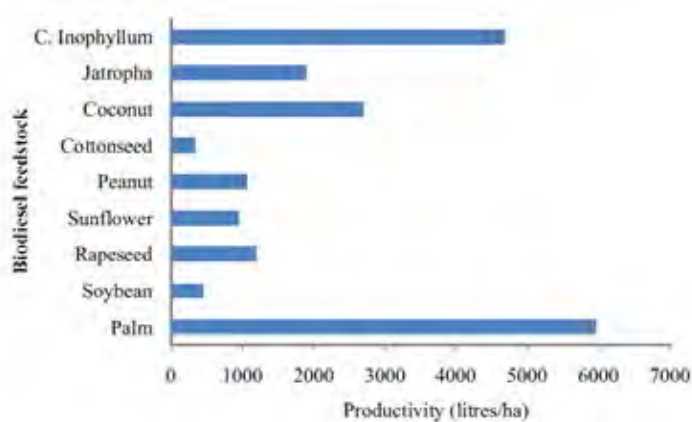


Figure 2.2 The production yield of oil from various sources biodiesel feedstock (Ong *et al.*, 2011).

Due to Malaysia and Indonesia is major producer of crude palm oil which produced around 17.5 million and 20.9 million metric tons, respectively in 2009. In refining process of the crude palm oil, low valuable product called “Palm fatty acid also known as PFAD” is generally generated in the fatty acid stripping then followed by deodorizer. Typically, PFAD is a common material for soap production, industry boiler fuel, animal feed industries, and also oleochemical industries such as candle factory. PFAD is mainly contains of free fatty acids approximate 85% up especially palmitic acid and oleic acid as major components as shown in Table 2.3. Moreover, PFAD is strongly recommended for biodiesel industries sources that have high potential to produce fatty acid methyl esters (FAMES) via esterification with the presence of methanol and catalyst.

Table 2.3 The properties of fatty acid distillates from palm oil

Fatty acid composition (FAC) of palm fatty acid distillate (PFAD)						
(weight % methyl ester)						
FAC	Range		Mean		S.D.	
	This study	Moh <i>et al.</i> (1999)	This study	Moh <i>et al.</i> (1999)	This study	Moh <i>et al.</i> (1999)
C8:0 capric	0-0.3	0-0.2	0.2	0.1	0.08	0.05
C10:0 caprylic	0-0.2	0-0.2	0.17	0.1	0.06	0.04
C12:0 lauric	0.1-2.4	0.1-1.7	0.46	0.4	0.61	0.30
C14:0 myristic	0.9-1.6	1.0-1.8	1.20	1.2	0.20	0.19
C16:0 palmitic	43.0-49.1	46.4-51.2	46.9	47.8	1.46	1.40
C16:1 palmitoleic	0.1-0.3	0.2-0.3	0.15	0.2	0.06	0.01
C18:0 steric	4.0-4.5	3.7-5.1	4.30	4.3	0.13	0.29
C18:1 oleic	34.7-37.2	33.0-37.7	36.7	1.13	1.13	1.41
C18:2 linoleic	8.5-9.7	7.8-9.6	9.03	0.28	0.28	0.45
C18:3	0.3-0.5	0.3-0.5	0.31	0.096	0.096	0.07
C20:0 arachidic	0.0-0.4	0.3-0.4	0.28	0.08	0.08	0.05
other	0-0.2	0-0.5	0.10	0.05	0.05	0.12

In 2014, Zuraida Wan and co-worker studied the production of FAME from PFAD via esterification using chromium–tungsten–titanium mixed oxides solid (CrWTiO_2) as catalysts. The reaction occurred in batch reactor at the range of temperature 110–200 °C. They investigated treatment conditions during catalyst preparation, parameters that had an affected on reaction, leaching of species and the recycled of catalyst.

In the result of this study, they found that the prepared catalyst CrWTiO_2 that had heat treated at 600 °C for 3 h calcination displayed the highest activity and stability compared to other prepared catalysts with different calcination parameters. The maximum 83% of FAME obtained from reaction condition at 170 °C for 3 hr. and 2 wt.% of catalyst quantities. Furthermore, the deactivation of CrWTiO_2 catalyst can be regenerated by heat treatment and effectively at four times recycled. Hence, the benefit of CrWTiO_2 catalyst is good activity at moderate reaction parameters, can be reusable with minimum leaching, and catalyst can prepared by a simple method.

Sikarin Tamiyakul *et al.* (2015) investigated the effect of Ga and Zn over H-ZSM-5 for aromatic production from palm fatty acid distillate (PFAD). They studied over H-ZSM-5, Ga/H-ZSM-5, and Zn/H-ZSM-5 catalysts at 500 °C, atmospheric pressure for 3 hr. The purpose of these reaction pathways were the deoxygenation of fatty acid via decarboxylation, decarbonylation, or directly cracking of fatty acid molecules, to produced long chain hydrocarbons (C11–C17) at first step. While the oxygenated compounds were deoxygenated via a decarboxylation and/or decarbonylation reaction and released CO_2 , CO, and H_2O . The long chain hydrocarbons were further cracked at by acid sites of H-ZSM-5, generating aliphatic hydrocarbons (C6–C10).

They demonstrated that the introduced of both Ga and Zn is promoted the aromatization of PFAD due to increasing dehydrogenation function. The higher aromatics yield of Zn/H-ZSM-5 was obtained by the presence of two zinc species; exchanged Zn^{2+} which promoting the dehydrogenation of paraffins and ZnO which promoting the decarboxylation of oxygenates. The shifting from decarbonylation to decarboxylation means shifting from the Brönsted acid site of the parent H-ZSM-5 to ZnO preserved the Brönsted acid site for aromatization, hence increasing the aromatics yield.

2.4 The Overall Reaction For Biojet Fuel Production

2.4.1 Hydrodeoxygenation

Hydrodeoxygenation is a process that removes oxygenated compounds from a molecule usually in the form of water using variety of catalysts for instance nickel-molybdenum, cobalt-molybdenum, and nickel-cobalt supported on alumina and zeolite materials where hydrogen is used to cleave carbon-carbon or carbon-heteroatom bonds in a molecule. The high oxygen content of vegetable oils plays a key role in fuel properties effects in term of low heating value, thermal and chemical instabilities, and corrosive. Therefore, vegetable oils that has the long chain glyceride esters contain carbonyl oxygens could be removed via hydrodeoxygenation.

There are several reaction pathways for straight-chain hydrocarbons production. In Figure 2.3 displayed hydrodeoxygenation reaction that can be occurred through three routes way: direct hydrodeoxygenation (HDO) which is the most desired route, decarboxylation, and decarbonylation. Generally, HDO reactions produce water when the C=O double bond is cleaved initially, result to the formation of alcohol. Furthermore, hydrogenation of C-O bond occur alkane formation. However, Fatty acids can be also directly decarboxylated or decarbonylated. During decarboxylation reaction, oxygen is removed in the form of CO₂ (carbon dioxide) by the direct attack at C-C single bond. In decarbonylation reaction, oxygen is removed in the form of water and CO (carbon monoxide). The product distribution is depends on their action route and catalyst type. Nevertheless, both decarboxylation and decarbonylation are not easy to split from each other due to CO₂, CO gases and the presence of hydrogen on the surface of the catalyst lead easy reaction occurs.

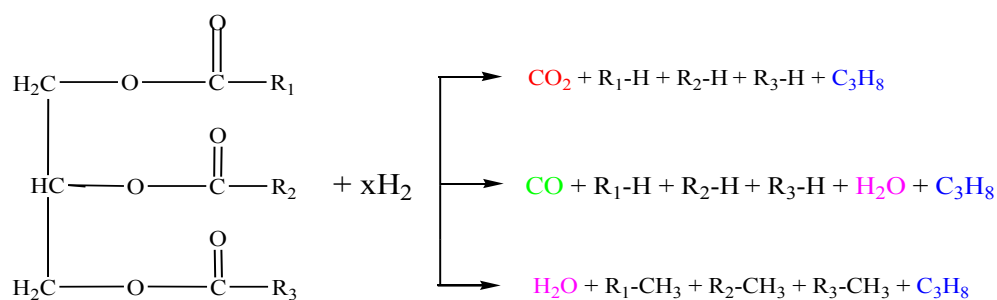


Figure 2.3 Main reactions occur in deoxygenation of triglycerides (Kordulis *et al.*, 2016).

The reaction factor such as the hydrodeoxygenation process, optimization of reaction temperature and hydrogen pressure, species of catalyst and catalyst loading is also essential have to design properly to achieve objective. Catalyst should be designed to avoid side reactions as most as possible and have higher selectivity towards to meet specific products.

The direct hydrodeoxygenation, oxygen molecules present in feedstocks react with hydrogen at high temperature in range of 250–400 °C and pressure approximate around 3–10 MPa which hydrocarbons are obtained as main products. Besides, the reaction activity of C=O, C=C, C–O and C–C bonds have been considered in different metal and supported (Dupont *et al.*, 2011).

Hydrocracking and hydroisomerization of *n*-paraffins are essential processes in refinery used to upgrade chemicals to become more valuable, for instance high-octane reformulated gasoline, diesel and lubricating oil. Hydroconversion reactions are efficiently carried out over bifunctional catalysts, consisting of a metal, which is performing hydrogenation–dehydrogenation reactions, and an acidic functionality, which is taking action on C–C and C–H bond activation. Accordingly, in order to promote the hydroisomerization reaction, different oxides, such as alumina, zirconia, and sulfides were applied to the reaction. Also, the zeolites (e.g., MOR, BEA, ZSM-5, MAZ, OFF, USY, ZSM-22, MCM-22), and zeolite-like solid acids (e.g., SAPO-11, AlPO-5, SAPO-41) have been used as acidic components together with a metal (i.e., Pt, Ni, Pd, Co, Mo, Ir, Ru, Rh, Re). Over zeolites, both process proceed through consecutive branching reactions (i.e.,

isomerization of *n*-paraffins), while cracking reactions occur in parallel with isomerization. (Santos *et al.*, 2011).

2.4.2 Hydrocracking

Hydrocracking is a catalytic chemical process used in petroleum refineries for converting the high-boiling constituent hydrocarbons in petroleum crude oils to more valuable lower-boiling products such as gasoline, kerosene, jet fuel, and diesel oil. The process takes place in a hydrogen-rich atmosphere at elevated temperatures (260–425 °C) and pressures (35–200 bar).

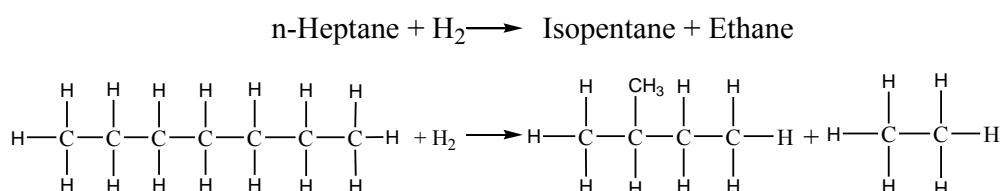


Figure 2.4 The schematic of hydro cracking reaction.

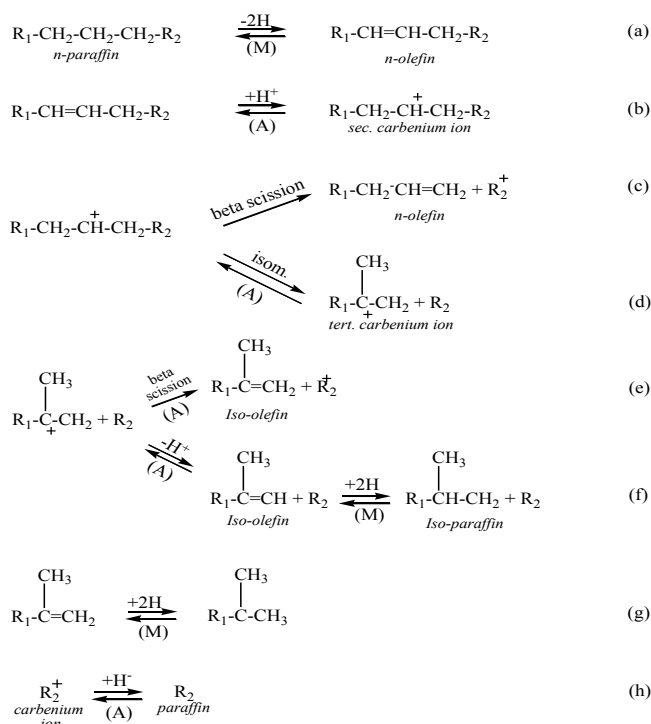
Hydrocracking of *n*-paraffins over a bifunctional catalyst goes through the following steps:

1. Adsorption of *n*-paraffins on metal sites
2. Dehydrogenation with formation of *n*-olefins
3. Desorption from metal sites and diffusion to acid sites
4. Skeletal isomerization and/or cracking of olefins on the acid sites through carbenium ion intermediates
5. Desorption of formed olefins from acid sites and diffusion to metal sites
6. Hydrogenation of these olefins (*n*- and *iso*-) in metal sites
7. Desorption of resulting paraffins

The proposed β -scission mechanisms suggest that the *n*-paraffins submitted to hydrocracking may undergo several isomerizations until a configuration is attained that is favorable to β -scission.

The cracking of isomers occurs preferentially near the center of the hydrocarbon chain and practically no methane or ethane formation is observed. For large carbenium ions, the cracking by β -scission is more likely to occur with dibranched and tribranched isomers than with monobranched ones. Furthermore, the cracking of lower molecular weight paraffins via β -scission is less likely to occur, which explains their high yields even at high conversions.

The elementary reactions corresponding to the reaction path explained are shown in Figure 2.5. Product analysis has shown that whenever several reaction pathways are possible, the one leading to the formation and subsequent cracking of a tertiary carbenium ion is preferred (reaction (d) and (e) in Figure 2.5). While the hydrogenation/dehydrogenation and isomerization reactions are reversible, the cracking reactions are irreversible.



A: acid site, **M:** metal site

Figure 2.5 Typical reaction path way in hydrocracking of *n*-paraffins.

The hydrogenation-to-acidity ratio is significantly effect on the hydrocracking of paraffin. The *iso*-to-normal ratio in product paraffin increases with decreasing reaction temperature because the cracking rate of *iso*-paraffins increases faster than that of *n*-paraffins at higher temperature. This is illustrated by the hydrocracking of *n*-decane in Figure 2.6. The *iso*-to-normal ratio also increases when the catalyst contains a weak hydrogenation component and strong acid component. The higher *iso*-to-normal ratio is attributed to a higher rate of isomerization of olefinic intermediates at the strong acidic sites.

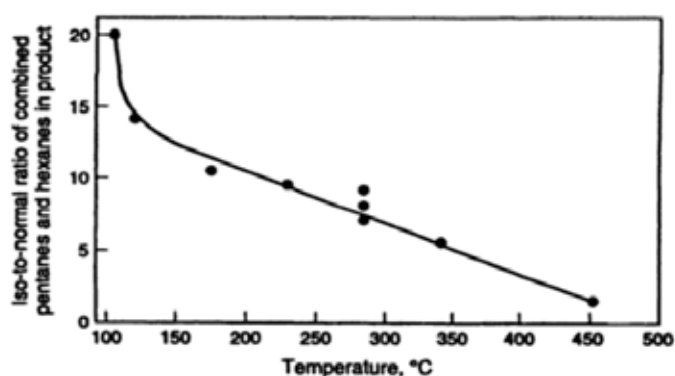


Figure 2.6 Effect of reaction temperature on *iso*-to-normal paraffin ratio in products obtained from hydrocracking of *n*-decane over strongly acidic catalyst.

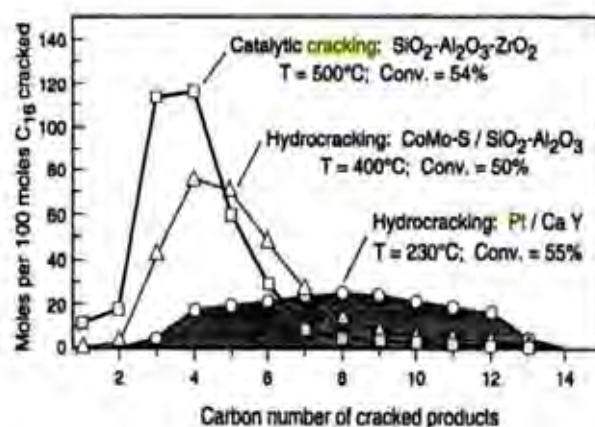


Figure 2.7 The distribution of carbon number in catalytic cracking and hydrocracking of *n*-hexadecane during 50% conversion.

Figure 2.7 displays the product distribution of *n*-hexadecane hydrocracking with catalysts having different hydrogenation components and different supports. A higher hydrogenation-to-acidity ratio in the catalyst was result in wider spread of products. Such hydrocracking is sometime called “ideal hydrocracking” and often results in higher liquid yields. In “Ideal hydrocracking,” the rate determining events (isomerization and β -scission) occur at the acid site, whereas the metal sites serve only for rapid hydrogenation and dehydrogenation.

A high rate of desorption and hydrogenation of the primary cracking products before secondary cracking implied to the wide spread of products. The high rate of carbenium ion desorption is due to their displacement by *n*-olefins, whose steady state concentration is higher in the presence of strong hydrogenation/dehydrogenation component (competitive sorption/desorption). The strength of this component can influence the rate of desorption of tertiary carbenium ion and product distribution. Figure 2.7, the long-chain molecule tends to crack in or near the center because C1 or C2 hydrocarbons were not found in product.

Anyway, the catalysts with low hydrogenation-to-acidity ratios, some of primary cracking reaction remains longer adsorbed at acid site and undergo secondary cracking. This results in higher yields in low molecular weight products (C2–C6). In low hydrogenation component, the secondary cracking reaction becomes more important and lead to high yield of low molecular weight products as illustrated in Figure 2.7.

Hydrocracking over a catalyst consisting of a strong hydrogenation component (e.g., platinum) and a weak acidic or non-acidic component proceeds via a hydrogenolysis mechanism on the metal. This is resulted in high yields of C1 and C2 hydrocarbons, along with *n*-paraffins, and a near absence of *iso*-paraffins. (Scherzer *et al.*)

2.4.3 Hydroisomerization

One conventional method for removal is isomerization of *n*-paraffins to isoparaffins. The isomerization process usually takes place in the presence of hydrogen, and in this case it is referred to as hydroisomerization (Deldari, 2005).

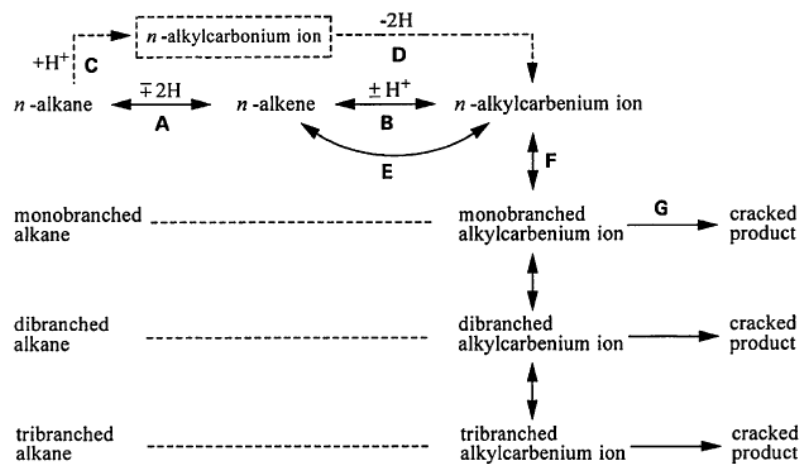
Isomerization reactions generally take place over bifunctional catalysts containing metallic sites for hydrogenation/dehydrogenation and acid sites for skeletal isomerization via carbenium ions. According to the classical isomerization mechanism, paraffins dehydrogenate on the catalyst metal sites, and the produced olefins protonate on the Brønsted acid sites to the corresponding alkylcarbenium ions. These carbenium ions undergo skeletal rearrangement and β -scission follows by deprotonation and hydrogenation over metal to the corresponding paraffins. The consecutive steps of this mechanism generally are as follows:

1. Dehydrogenation on the metal;
2. Protonation of olefins on the Brønsted acid sites with formation of a secondary alkylcarbenium;
3. Rearrangement of the alkylcarbenium ion via formation of cyclic alkylcarbenium type transition state (PCP mechanism);
4. Deprotonation;
5. Hydrogenation.

Figure 2.8 illustrates the bi-functional pathways of hydroisomerization and cracking of *n*-paraffins. Generally acidic supports of bi-functional catalysts are occurred as follows:

1. Amorphous oxides or mixture of oxides (i.e. Al_2O_3 , $\text{SiO}_2\text{-Al}_2\text{O}_3$, $\text{ZrO}_2/\text{SO}_4^{2-}$)
2. Zeolites (Y, Beta, Mordenite, ZSM-5, ZSM-22)
3. Silicoaluminophosphates (SAPO-11, SAPO-31, SAPO-41)
4. Mesoporous materials (MCM-41, AIMCM-41 (Deldari, 2005))

The most common used metals species for making this kind of catalysts are Pd, Pt and Ni bimetallic systems whereas zeolites are widely used acid catalysts. A several range of zeolites such as ZSM-12, Y-zeolite, SAPO-11, MCM-41, SBA-15 and ZSM-22 have been applied to the hydroisomerization.



A : Hydrogenation-dehydrogenation on metallic sites.

B : Protonation-deprotonation on acid sites.

C : Addition of proton to form alkylcarbonium ion on acid sites.

D : Dehydrogenation to form alkylcarbenium ion.

E : Competitive adsorption-desorption of alkene and carbenium ion on acid sites.

F : Rearrangement of alkylcarbenium ion.

G : Cracking of alkylcarbenium ion.

Figure 2.8 The bi-functional pathways of hydroisomerization and cracking of *n*-paraffins.

In 2013, Hyung Won Lee *et al.*, studied hydroisomerization of *n*-dodecane over Pt/Y zeolites with different acid characteristics which *n*-dodecane is a model reactant for producing jet-fuel from FT-wax. They used several range of acid of Y zeolites composed of NaY, HY ($\text{SiO}_2/\text{Al}_2\text{O}_3 = 5.1$), HY ($\text{SiO}_2/\text{Al}_2\text{O}_3 = 80$), and HY ($\text{SiO}_2/\text{Al}_2\text{O}_3 = 200$). The acidity in each Y zeolites was modified by followed: NaY was ion exchanged with NH_4Cl , HY ($\text{SiO}_2/\text{Al}_2\text{O}_3 = 5.1$) and HY ($\text{SiO}_2/\text{Al}_2\text{O}_3 = 80$) were silylated. Pt was impregnated zeolite Y catalysts at various $\text{SiO}_2/\text{Al}_2\text{O}_3 = 5.1$ ratio values, NaY (5.1), HY (5.1), HY (80), and HY (200), were applied to hydroisomerization reaction of *n*-dodecane. The effects of temperature and pressure in the catalytic activity were also investigated.

They reported that the conversion of *n*-dodecane decreased with increasing SiO₂/Al₂O₃, whereas selectivity of isomerization increased with increasing SiO₂/Al₂O₃ in all the modification Y zeolites (both acidity control by ion-exchange and silylation ways). In addition, HY (SiO₂/Al₂O₃ = 80) revealed the best hydroisomerization activity. In a result of varied temperature in the range of 280–360 °C under a constant pressure of 40 bar, the conversion increased and the selectivity decreased with increasing temperature. However, with increasing pressure were dropped down the isomerization efficiency due to when increased pressure, the adsorption of *n*-dodecane on the active sites of the catalyst was prevented by hydrogen molecules that compete with *n*-dodecane. When they improved the catalyst by impregnated metal with the range of 0.1–1.0%, they obtained that yield of *iso*-dodecane slightly increased with increasing metal concentration but the effect was not large. They were suggests that the effect of the acid sites is greater than that of the impregnated metal.

2.4.4 Hydrogenation and Dehydrogenation

In the petroleum industry, several processes involved in the manufacture of gasoline and petrochemical products are based on the destructive hydrogenation of hydrocarbons.

Hydrogenation is a chemical reaction between molecular hydrogen (H₂) and another compound or element, usually in the presence of a catalyst such as platinum, palladium or nickel. The process is commonly employed to reduce or saturate organic compounds. Hydrogenation typically constitutes the addition of pairs of hydrogen atoms to a molecule, generally an alkene. Catalysts are required for the reaction to be usable; non-catalytic hydrogenation takes place only at very high temperatures. Hydrogenation reduces double and triple bonds in hydrocarbons

The industrial importance of the hydrogenation process dates from 1897, when Sabatier encountered that the introduction of a trace of nickel as a catalyst facilitated the addition of hydrogen to molecules of carbon compounds.

The successful performance of a catalytic hydrogenation depends on a suitable choice of reaction conditions, in particular, the choice of catalyst and its

amount, temperature, hydrogen pressure, and solvent. Hydrogenation catalysts are also subject to deactivation or promotion by various substances that are referred to as inhibitory (or poisons) or promoters, respectively. In some case, the impurities of the substrate to be hydrogenated or the product may become a factor that retards the hydrogenation, usually in a later stage of the reaction (Nishimura).

The dehydrogenation of hydrocarbons involves the breaking of two carbon-hydrogen bonds with the simultaneous formation of a hydrogen molecule and a molecule containing a double carbon-carbon bond, which usually represents the desired product. The double bond is a highly reactive point that permits the use of molecules which contain it as intermediates for the production of typical petrochemical products such as polymers.

2.4.5 Hydrogenolysis

Hydrogenolysis is a chemical reaction whereby a carbon-carbon or carbon-heteroatom single bond is cleaved or undergoes lysis (breakdown) by hydrogen. The heteroatom may vary, but it usually is oxygen, nitrogen, or sulfur. A related reaction is hydrogenation, where hydrogen is added to the molecule, without cleaving bonds. Usually hydrogenolysis is conducted catalytically using hydrogen gas (Connor *et al.*, 1932). The following scheme is represents the hydrogenolysis reaction:

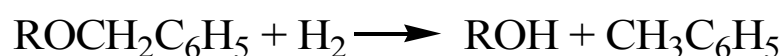


Figure 2.9 Schematic of hydrogenolysis reaction (Connor *et al.*, 1932).

2.5 Catalyst For Biojet Production

Many important hydrocarbon reaction such as paraffin cracking and isomerization, are catalyzed by material with acid properties. Some reactions require sites of stronger acidity than others, for example, in paraffin cracking, the required strength of the acid sites is stronger than that required for isomerization. When the

metallic function is added to the acid function, a bifunctional catalyst is obtained. This catalyst presents in general a more beneficial behavior than the catalyst having only the acid function. The bifunctional metal-acid catalysts are generally porous oxides with acid properties that have a small amount of a metal support on them. The acid function of support and the metal function may be tuned to promote the desired reaction selectivity by the addition of promoters (Borghet, 2010).

2.5.1 Core-shell Catalyst

Core-shell nanostructures are nanoparticles encapsulated and protected by an outer shell that isolates the nanoparticles and prevents their migration and conjugation during the catalytic reactions. An efficient of core-shell catalysts requires porous shells that can allow free access of chemical species from the outside to the surface of nanocatalysts.

In 2012, Okada *et al.* investigated the structural design of heterogeneous catalysts for one-pot reaction. The series of core-shell catalysts were synthesized which consisted of SiO₂ core, Pd nanoparticles (NPs), and Ti containing mesoporous silica (Ti-MS) shell with precise control of the Pd NPs positions, the mesopore diameter, and the thickness of the Ti-MS shell. The catalytic potentials were evaluated for one-pot oxidation reactions involving the direct synthesis of hydrogen peroxide (H₂O₂) from H₂ and O₂ gases by the Pd NPs and the subsequent oxidation reaction of sulfide by the isolated Ti IV species using in situ produced H₂O₂ in the mesoporous silica.

Considering a series of core-shell catalysts consisting of a SiO₂ core, Pd NPs, and a Ti-MS shell were prepared, and their effect on the one-pot oxidation of sulfides was investigated. The position of the deposited Pd NPs was investigated first to clarify the benefit of the core-shell structure. The diameter of the mesoporous channels and the thickness of the Ti-MS shell were controlled to improve the activity and examine the enhancement mechanism. The core-shell structure was also found to have an effect on not only the catalytic activity, but also on the product selectivity.

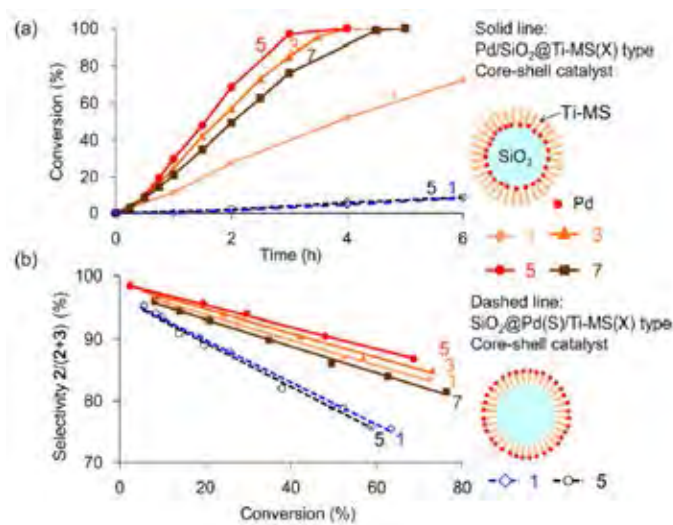
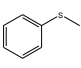
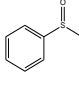
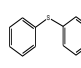
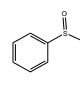


Figure 2.10 (a) Kinetics of methyl phenyl sulfide one-pot oxidation and (b) dependence of the conversion level on the selectivity using Pd/SiO₂@Ti-MS or SiO₂@Pd(S)/Ti-MS type core-shell catalysts with various shell thicknesses (different amounts of precursors; 1, 3, 5, and 7 times the original amount) (Okada *et al.*, 2012).

From Figure 2.10 Okada *et al.* (2012) demonstrated that the activity and selectivity of the Pd/SiO₂@Ti-MS type core-shell catalyst increased with increasing shell thickness and were maximized at a thickness of 155 nm. It is considered that shell thickness of approximately 35 nm is not sufficient to utilize the in situ generated H₂O₂, and the efficiency of H₂O₂ within the mesoporous channels was even further enhanced by increasing the shell thickness due to the suppression of reactant dispersion to the solvent. However, further increase in thickness to 185 nm decreased the catalytic activity and selectivity, which is ascribed to the retardation of diffusion with a thicker mesoporous silica shell.

Table 2.4 Summary of catalyst sample parameters, activity, and selectivity for one-pot oxidation (Okada *et al.*, 2012)

Sample parameter						Substrate/Product			
									
Core-shell type	Pd position	SDA	Pore diameter (nm)	Amount of precursor	Shell thickness (nm)	Activity	Selectivity	Activity	Selectivity
Pd/SiO ₂ @Ti-MS	Boundary	C ₁₂ TABr	1.9	1	28	1.8	84	0.6	61
	Boundary	C ₁₄ TABr	2.3	1	30	2.6	86	1.2	75
	Boundary	C ₁₆ TABr	2.6	1	33	6.0	87	4.3	80
	Boundary	C ₁₈ TACl	2.9	1	35	11.2	88	6.3	83
	Boundary	C ₁₈ TACl	2.8	3	105	28.4	89	27.4	84
	Boundary	C ₁₈ TACl	2.8	5	155	32.3	90	40.7	87
	Boundary	C ₁₈ TACl	2.7	7	185	24.8	87	14.9	80
SiO ₂ @Pd(S)Ti-MS	Outer surface	C ₁₆ TABr	2.1	1	30	1.6	72	1.8	61
	Outer surface	C ₁₈ TACl	2.2	1	32	1.5	79	1.4	67
	Outer surface	C ₁₈ TACl	2.5	5	115	1.5	80	1.9	69
SiO ₂ @Pd(R)Ti-MS	Random	C ₁₆ TABr	2.0	1	30	2.0	78	2.9	71

Activity = [moles of sulfide converted]/[hour-moles of Pd]
 Selectivity = [moles of sulfoxide]/[moles of sulfoxide + sulfone] × 100 (at conversion of sulfide = 50%)

In Ramya 2012 *et al.* studied the production of liquid hydrocarbon fuels from jatropha oil through catalytic cracking technology using AlMCM-41/ZSM-5 composite catalysts. They had developed of mesoporous catalysts with large pore opening that facilitates the entry of bigger molecules but they suffer from their low acidic nature and poor hydrothermal stability with small pore openings make it difficult for the entry large molecules such as triglycerides in the model of core-shell catalyst. The advantages of the combination of these micro and mesoporous materials in these composite catalysts was improved the yield of Bioliquid fuel and the selectivity towards green gasoline up to 70% with 100% conversion.

2.5.2 Zeolite

Zeolites are solid crystalline of aluminosilicates, which consist of SiO₄ and AlO₄- tetrahedral, and interlinked to be three dimension network of porous

structure. They can be built by nature or synthesis. Inside of zeolites pore have metals or other cations, which balance negative charge from the anionic framework resulting from the containing aluminium. The general formula of zeolite is $M_v(\text{AlO}_2)_x(\text{SiO}_2)_y \cdot z\text{H}_2\text{O}$; where M are metal cations. The composition of zeolites are identified by the Si/Al atomic ratio or by molar ratio M ($M = \text{SiO}_2/\text{Al}_2\text{O}_3$)

The zeolites growth can be shown in Figure 2.11. The SiO_4 and AlO_4 -tetrahedral, which is defined as primary units are polymerized to planar secondary units, then evolve to complex three-dimension unit called polyhedral e.g. cube, hexagonal and octahedral. These polyhedral are ultimately arranged in many connection modes to form porous structure (cages and channels) of zeolites such as sodalite cage and supercage.

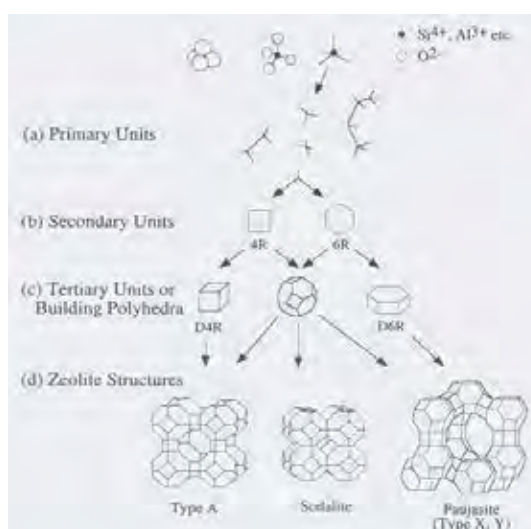


Figure 2.11 Formation of three common zeolites from primary units.

The pore of zeolites can be oriented in one, two or three dimension (Figure 2.12) and aperture of pore depend on number of T-atom composition (Si, Al, or other metals; (see Table 2.5). The pore size can be changed by exchanging the cation in zeolites: for example, the aperture size of zeolites A can be modified to be 3, 3.8 and 4.3 Å when use K^+ , Na^+ , and Ca^{2+} as balancing cation, respectively (Bartholomew *et al.*, 2005 and Hagen, 1999).

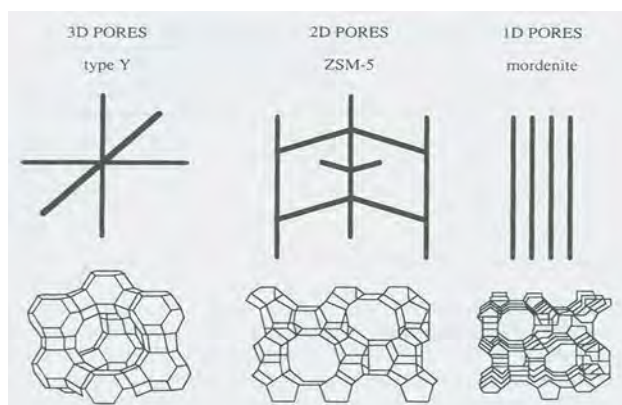


Figure 2.12 Three commercial zeolites of difference dimensionalities.

Table 2.5 Zeolites classified by window size (Sooknoi)

Types	Small	Medium	Large	Extra large	Mesopore
Pore size (nm)	0.4 - 0.5	0.5 - 0.6	0.7 - 0.8	1.0 - 1.4	>2.0
T-atom	8	10	12	14-20	Variable
	Zeolite A	ZSM-5	Faujasite	CIT-5	MCM-41
	Chabasite	Theta-1	Cancrinite	VPI-5	MCM-48
	Rho	Ferrierite	Mordenite	Cloverite	
	Erionite	ZSM-11	Zeolite L		
	Zeolite P	ZSM-23	Offretite		
	Analcime		Beta		
	Phillipsite		Gmelinite		

2.5.2.1 Zeolite HY

The observed differences in activity were attributed to differences in zeolite pore geometry: whereas Pt/HY and Pt/H-ZSM-5 have a three-dimensional pore network that facilitates the diffusion of feed and product molecules, mordenite has one-dimensional pores. In mordenite, the pores can be easily blocked by platinum or coke, reducing catalyst activity and leading to rapid deactivation.

However, zeolite-based catalysts exhibit lower activity and thus the reaction must be performed at higher temperature (250 °C), favoring unwanted cracking side reactions. Great efforts have been directed to modify zeolite supports in these catalysts via strengthening or creating stronger acid sites, compared to the traditionally used alumina support, as well as modifying the metal sites via incorporating metallic promoters.

Among the zeolites, USY has been tested successfully. USY consists of a highly hydrothermal steam Faujasite (FAU) type Y dealuminated zeolite having a secondary porosity obtained during the partial destruction of the zeolite, which results in the formation of mesopores. The so-called ultra-stable FAU type Y zeolite (e.g., USY) is responsible for the facilitation of the diffusion of larger molecules into zeolite channels, which is a pre-requisite of the hydroconversion application.

Zeolite Y is a faujasite molecular sieve with 7.4 Å diameter pore and a three-dimensional pore structure. The basic structural units for zeolites Y are the sodalite cages, which are arranged so as to form supercages that are large enough to accommodate spheres with 1.2 nm.

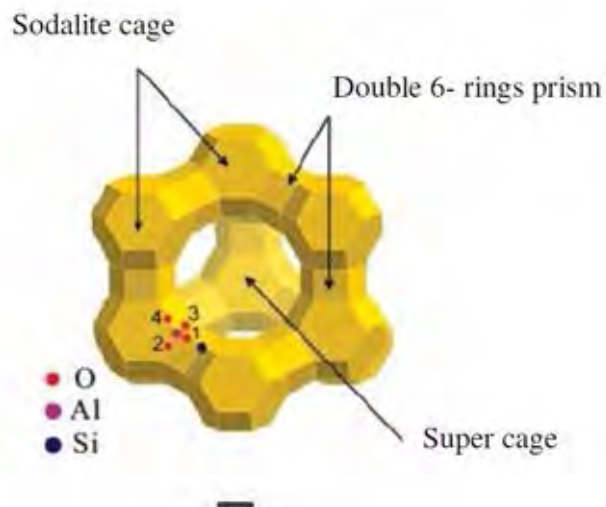


Figure 2.13 The 3D illustrate of Y zeolite structure. The silicon or aluminum ions are located at the corners and the oxygen ions near the edges.

Figure 2.13 is shown Y zeolite structure. Each supercage contains four windows of 12-membered Al or Si rings with a diameter of 7. Å. while the diameters of the sodalite cage and the double 6-ring are 6.6 and 2.6 Å respectively.

Recently, Y zeolite has been found to exhibit good catalytic performance for catalytic process because of its unique properties, for instance the main pore structure is uniform three-dimension with widely pore opening enough to admit the large molecules, excellent flexibility structure to control Al content of the structure for possible to optimize active catalyst, high thermal and hydrothermal stability in order to withstand regenerate conditions. However, the synthesis of Y zeolite is a complex process, due to the complexly growth of pure crystal of Y zeolite is very sensitive to preparation condition. Furthermore the poor crystal has negative effect to the performance of Y zeolite catalyst.

2.5.3 Titanium Dioxide

Titanium dioxide TiO_2 is a semiconductor oxide, for which four different polymorphs exist at normal conditions: rutile or anatase. Even if anatase has better chemical properties, including those related to photochemistry, rutile is easier to model from a computational point of view. Rutile is also the ground state under ambient conditions although for small crystallites the lower surface energy of the anatase faces with respect to those of rutile can lead to formation of anatase quite frequently using some preparations. Rutile has a layered structure and the (110) surface is non-polar in nature and was one of the first oxides where STM measurements were successfully carried out and the images simulated through the use of theoretical methods and the Tersoff-Hamann formalism.

Medium-to-high surface area anatase is largely used as support of catalysts. The instability of anatase toward phase transformation into rutile does not allow its use for high-temperature reactions. In case of reaction temperatures 300-400°C normal high-area anatase may be used, in particular when anatase stabilizing components (such as silicate, molybdate, wolframate species or alkali or rare-earth ions) are also present. Mesoporous very high surface-area anatase may offer good opportunity for relatively low-temperature reactions such as, e.g., low-temperature CO oxidation over titania-supported noble metals. (Busca *et al.*)

In 2012, Bovornseripatani and co-worker studied the production of hydrogenated biodiesel over Pd/TiO₂ from various biomass such as beef fat, chicken fat, pork fat, and jatropha oil. The reaction was tested in a continuous flow packed-bed reactor at 500 psig, 325 °C, H₂ /feed molar ratio of 30, and LHSV of 4 h⁻¹ for its catalytic activity and selectivity in hydrodeoxygenation.

They found that *n*-pentadecane (*n*-C15) and *n*-heptadecane (*n*-C17) from the decarboxylation/decarbonylation reaction were main products of all feedstocks. The conversion of triglycerides in jatropha oil was higher than those of chicken fat, pork fat, and beef fat, respectively. The higher concentration of metal impurities in the feedstock brought the conversion of triglycerides dropped down because of the deposition of impurities on the catalyst surface. Furthermore, the

higher concentration of phosphorus gave the higher coke deposition due to the oligomerization.

Cheng *et al.* (2014) investigated the optimizing catalysis conditions to decrease aromatic hydrocarbons and increasing alkanes for improve jet biofuel quality. Ni and Mo clusters supported on zeolites HZSM-5 and HY catalysts were prepared using a wetness impregnation method for convert soybean oil into jet fuel.

They described that zeolite HY exhibited higher 40.3% jet range alkane selectivity and lower jet range aromatic hydrocarbon to 23.8% selectivity than zeolite H-ZSM-5 which 13.8% and 58.9% of jet alkane and jet aromatic selectivity respectively. The high alkane and low aromatic hydrocarbon selectivity of zeolite HY was attributed to its pore structure. Zeolite HY displayed 12-member ring pores which larger than lead large molecules such as fatty acids initially cracked into long chain alkanes in the cages or on the outer surface. Then, the long chain carbon alkanes after the crack were able to diffuse in the pores of zeolite HY or be further cracked into short chain alkanes inside the pore. Nevertheless, zeolite HZSM-5 contained only 10-member ring pores (small pore size) cannot lead large molecules access to the micropores thus it had to be pre-cracked into alkanes on the outer surface of zeolite H-ZSM-5. It can be concluded that zeolite H-ZSM-5 were not allow large alkanes to diffuse until they cracked into aromatic hydrocarbons with shorter carbon chains. When reaction temperature increased from 330 to 390 °C, yield of jet fuel over Ni–Mo/HY catalyst at hydrogen pressure 4 MPa increased from 0% to 49.1% due to the shift of reaction pathway from oligomerization to cracking reaction. Besides increase of reaction temperature from 390 to 410 °C resulted in increased yield of jet range aromatic hydrocarbons from 18.7% to 30%, which decreased jet fuel quality. The best condition of high jet fuel yield around 48.2% was obtained at hydrogen pressure 1 MPa over Ni (8 wt.%)–Mo (12 wt.)/HY catalyst due to decarbonylation pathway required less hydrogen for reaction to be occurred.

2.5.4 Metal Catalyst

For several industrial zeolites is basically used as hydroisomerization catalysts, which provide the acid function. As the hydrogenating-dehydrogenating function, various species of metals have been tested including Pt, Pd, Rh, Ir, Ru, Re and Ni, mostly associated with mordenite or CaY. Bifunctional catalysts, with both hydrogenating/dehydrogenating and isomerization function have shown high efficiency in alkane hydroisomerization. Noble metal-zeolite catalysts especially Pt or Pd loaded Y, mordenite, and beta leads a high activity and selectivity for hydroisomerization of *n*-alkanes (Lucas *et al.*, 2006).

Nickel is a very active metal in hydrogenation catalysis. It is also a cheap element thus allowing its use as a bulk metal (e.g. as Raney nickel) as well as in the form of highly loaded supported catalysts. This also gives rise to some sulfur resistance, just because much sulfur is needed to fully poison highly loaded catalysts. On the other hand, the carcinogenic toxicity of nickel compounds is a big concern in the preparation and disposal of catalysts.

Many investigators have recognized that nickel oxide when supported on kieselguhr gives much more active catalysts than an unsupported one, although the reduction temperature required for the supported oxide (350–500 °C).

Selective deoxygenation of stearic acid and Microalgae oil over nickel catalysts supported on two types of zeolites (H-ZSM-5 and H-Beta) of varying Si/Al ratio using a batch reactor was studied by Peng *et al.* (2011). Full conversion of stearic acid was obtained over 10% Ni/H-ZSM-5 (Si/Al = 45) catalyst, but severe cracking of the produced alkanes (43% selectivity to C17 and C18) was observed own to its high acidity. However, using 10% Ni/H-ZSM-5 with higher Si/Al ratios (120 or 200), thus lower acidity, the cracking was gradually suppressed and the selectivity to C17 and C18 alkanes increased to 84 and 93%. For Ni/Beta catalysts with a higher Ni content (10 wt.%, Si/Al=75) displayed a similar activity as the former catalyst, but showed a lower selectivity to isomerized alkanes, indicating that its lower acid site concentration causes a lower isomerization rate. The hydrotreated microalgae oil converted over a 10% Ni/H-Beta catalyst (Si/Al = 180), the yield of saturated fatty acids were the primary products for microalgae oil conversion, that is

stearic acid exceeded 70 wt.% within 1 hr. After that, the yield of saturated fatty acids slightly decreased accompanied with an increase in alkane yields (mainly including C17 and C18 alkanes) as a function of time.

CHAPTER III EXPERIMENTAL

3.1 Materials and Equipment

3.1.1 Materials

3.1.1.1 *Feedstock*

- Palm fatty acid distillate

3.1.1.2 *Chemical Reagents*

- HY zeolite (SiO₂/Al₂O₃ ratio of 100, Tosoh Company)
- Nickle (II) nitrate hexahydrate (Ni(NO₃)₂•6H₂O, 99.99 %, Aldrich)
- Palladium chloride (PdCl₂)
- Acetylacetone (ACA, CH₃COCH₂COCH₃)
- Tetraisopropyl orthotitanate (TIPT, Ti(OCH(CH₃)₂)₄)
- Dodecylamine (CH₃(CH₂)₁₀CH₂NH₂)
- Acetone (CH₃COCH₃)
- Dichloromethane (CH₂Cl₂)
- Ethanol (C₂H₅OH)
- Hydrochloric acid (HCl)
- Deionized water
- Pyridine (C₅H₅N, 98 % purity, Carlo Erba)
- N,O-bis(trimethylsilyl)-trifluoro acetamide (BSTFA, C₈H₁₈F₃NOSi₂, 99 % purity, ACROS)

3.1.1.3 *Gases*

- Hydrogen (99.99% purity, BIG)
- Nitrogen (99.99% purity, Linde)
- Helium (99.99% purity, Linde)
- Air zero (99.99% purity, Linde)

3.1.2 Equipment

- High pressure packed-bed continuous flow reactor system;
- Mass flow controller (Brooks instrument 5850E)
- Teledyne ISCO syringe pumps 1000D
- Back pressure regulator (SIEMENS)
- $\frac{3}{4}$ " O.D.x16" long stainless steel reactor
- Three-zone tubular furnace with a temperature controller (Cabolite)
- Gas chromatograph (Agilent GC 7890 equipped with injector, DB-5 column and FID)
- Shimadzu GC-17A gas chromatograph equipped with a capillary HP PLOT/Al₂O₃ "S" deactivated column and FID detector
- Gas chromatograph-Simulated Distillation (Varian/ CP-3800)
- Oven
- Temperature programmed reduction (TPR) apparatus
- Temperature programmed desorption (TPD) apparatus
- Temperature programmed oxidation (TPO) apparatus
- X-ray diffractometer (XRD, Rigaku/ Smartlab)
- X-ray photoelectron spectroscopy (XPS, AXIS ULTRA DLD)
- Transmission electron microscopy (TEM)
- Surface area analyzer (SAA, Quantachrome/Autosorb-1)
- Gas chromatography with time-of-flight mass Spectrometer (GC-TOFMS)

3.2 Experimental Procedures

3.2.1 Preparation of 5 wt.% Ni Supported HY Catalyst

The zeolite Y was dried on an oven at 110 °C overnight. Then the dried zeolite was calcined at 500 °C for 3 h (heating rate 10 °C/min) for remove an impurity.

The nickel precursor solution was prepared by dissolved 0.8184 g of $\text{Ni}(\text{NO}_3)_2 \cdot 6\text{H}_2\text{O}$ in 6 mL of deionized water. After that, the zeolite was loaded by nickel metal solution by incipient wetness impregnation method. The mixture was gradually dried in an oven at 110 °C to remove excess water for 12 h. Then the dried nickel supported was calcined at 500 °C 4 h (heating rate of 10 °C/min).

3.2.2 Core-shell Catalyst Preparation

3.2.2.1 *Preparation of 5 wt.% Ni Supported HY Catalyst*

The nickel supported HY core-catalyst was also prepared by using the same procedure that is already described above.

3.2.2.2 *Preparation of Ni/HY^{Core}-Pd/TiO₂^{shell} Catalyst*

ACA (Acetylacetonone) was first introduced into TIPT (tetraisopropyl orthotitanate) with and equal of mole ratio in order to moderate the hydrolysis and condensation processes of titanium precursor species. The solution is mixed until homogeneous mixing. Then 0.1 M LACH aqueous solution which behaving as a mesopore directing agent was added into the ACA-modified TIPT solution in order to control the porosity of the TiO₂. The mixture is continuously stirred at 40 °C overnight until obtained transparent yellow sol obtained.

An amount of palladium chloride solution is introduced to obtain the desire 1wt.% Pd in order to incorporate into the aged transparent sol solution. The resultant mixture was further aged at 40 °C for 30 min to acquire a homogeneous solution. The gel was formed by heating the sol solution into the oven at 80 °C overnight to attain completed gel formation. Subsequently, Ni/HY catalyst is introduced into the gel and stirred until the solution was homogeneous. After that, the gel was dried at 80 °C overnight.

Finally, the dried gel was calcined at 500 °C for 4 h to remove the LAHC template. Accordingly, the desired catalyst was obtained.

3.3 Catalyst Characterization

3.3.1 X-ray Diffractometer (XRD)

X-ray diffraction was used to determine the information about crystalline phase of synthesized catalyst by a Rigaku X-Ray diffractometer, RINT-2200 with Cu tube for generating CuK α radiation (1.5406 Å) and operating condition of 40 kV. The sample was measured in the 2 θ range of 5–80° with a scanning rate of 5 °/s.

3.3.2 X-ray Photoelectron Spectroscopy (XPS)

The chemical elements on the surface of catalysts were investigated by X-ray photoelectron spectroscopy (AXIS ULTRA DLD). Each chemical element produces the XPS peaks at characteristic binding energy values which identify each element that contains on the surface of the catalysts.

3.3.3 Brunauer-Emmett-Teller (BET)

The surface areas of the fresh and spent catalysts were measured by BET surface area analyzer (Quantachrome/Autosorb-1). The sample was first outgassed to remove the humidity and volatile adsorbents adsorbed on surface under vacuum at 150 °C for 4 h prior to the analysis. Then, N₂ was purged to adsorb on surface, measuring the quantity of gas adsorbed onto or desorbed from their solid surface at some equilibrium vapor pressure by static volumetric method. The solid sample was maintained at a constant temperature of the sample cell until the equilibrium is established. This volume-pressure data will be used to calculate the BET surface area.

3.3.4 Temperature Programmed Reduction (TPR)

Temperature programmed reduction was employed for evaluating the quantity of the reducible species present in the prepared catalyst and the temperature,

at which the reduction itself takes place as a function of temperature. In each test 50 mg of catalyst was placed in a 1/4" O.D. quartz tubular reactor, and heated (10 °C/min) under a He flow up to 500 °C, and held at the temperature for 3 h in order to remove moisture from the catalyst surface. The sample was cooled down to 30 °C. Then, the sample would be exposed to a stream of 5% H₂/Ar with a flow rate of 20 ml/min. After that, the sample was heated to 800 °C with a heating rate of 10 °C/min. The amount of hydrogen consumed was monitored on-line by an SRI model 110 TCD detector as a function of temperature.

3.3.5 Temperature Programmed Desorption (TPD) of Isopropylamine

The acidity of prepared catalysts was determined by the amine TPD technique. First, 50 mg of sample was reduced at 500 °C in a flow of H₂ for 3 hr. After reduction, the sample was cooled in H₂ to room temperature and then isopropylamine was injected in to sample. After removing the excess isopropylamine, the sample was linearly heated in He to 800 °C at a heating rate of 20 °C/min. Masses 44, 41, and 17 were monitored to determine the evolution of isopropylamine, propylene, and ammonia, respectively.

3.3.6 Temperature Programmed Oxidation (TPO)

This technique was employed to analyze the amount and characteristics of the coke deposited on the catalysts during reaction. TPO of the spent catalysts was performed in a continuous flow of 2% O₂ in He while the temperature was linearly increased with a heating rate of 12 °C/min. The oxidation was conducted in a 1/4" quartz fixed-bed reactor after the spent catalyst was dried at 110 °C overnight, weighed (30 mg), and placed between two layers of quartz wool. The sample was further purged at room temperature by flowing 2% O₂ in He for 30 min to stabilize the signal before starting a run. The CO₂ produced by the oxidation of the coke species was converted to methane using a methanizer filled with 15% Ni/Al₂O₃ and operated at 400 °C in the presence of H₂. The evolution of methane was analyzed using an FID detector.

3.3.7 Transmission Electron Microscopy (TEM)

The morphology of prepared catalyst was observed by a transmission electron microscopy (JEM-2100). For TEM analysis, the catalyst was dilute in the appropriate solvent, sonicated, and dry in the copper grid at room temperature.

3.3.8 Gas Chromatography with Time-of-Flight Mass Spectrometer (GC-TOFMS)

The unknown samples was analyzed using gaschromatrography-mass spectrometry method provides the significant advantage for determininig all of polar and non-polar chemicals. The prepared product sample from catalytic reaction was analyzed by Leco Pegasus 4D GC×GC-TOFMS following GC conditions:

Inlet: Splitless
Detector: Mass spectrometry
Column: 60 m long × 0.25 mm internal diameter, and 0.25 μm film thickness, capillary Rxi-PAH column.
Gas: Carrier: Helium 1 mL/min
Temperature: Injection port: 300 °C
Injection ratio: 10:1 split
Oven program: The primary oven condition were: 50 °C for 5 min, ramped at 10 °C/min to 169 °C, hold time 10 min. The tertiary programming was ramped at 20 °C/min to 340 °C, hold time 30 min. The transfer line temperature was 300 °C and the MS source temperature was set to 250 °C.

3.4 Catalytic Activity Testing

The schematic of the reactor system and the description of flow-diagram are shown in Figure 3.1 and Table 3.1, respectively. The hydrodeoxygenation, hydrocracking, and hydroisomerization reaction of palm fatty acid distillate were carried through 3/4" O.D., continuous flow fixed-bed reactor under high hydrogen pressure conditions. Firstly, the catalyst was reduced under flowing H₂ for 3 h at the reduction temperature of catalyst. After that, the temperature and pressure of the reactor were set to the desired value in a flowing H₂. Then, the stream of PFAD was fed into the reactor by teledyne isco syringe pumps 1000D. The flow of carrier gas and the reaction pressure were controlled by a mass flow controller and a back pressure regulator, respectively.

The liquid product was trapped and collected in a condenser while the gas product was analyzed online by using a Shimadzu GC-17A gas chromatograph equipped with a capillary HP-PLOT/Al₂O₃ "S" deactivated column and FID detector. Amount of gas product was corrected by using wet test gas meter (Ritter TG 05/2). Finally, the liquid product was analyzed by another gas chromatograph, Agilent 7890 equipped with a DB-5HT column and FID detector. Both gas product and liquid product were collected and analyzed hourly.

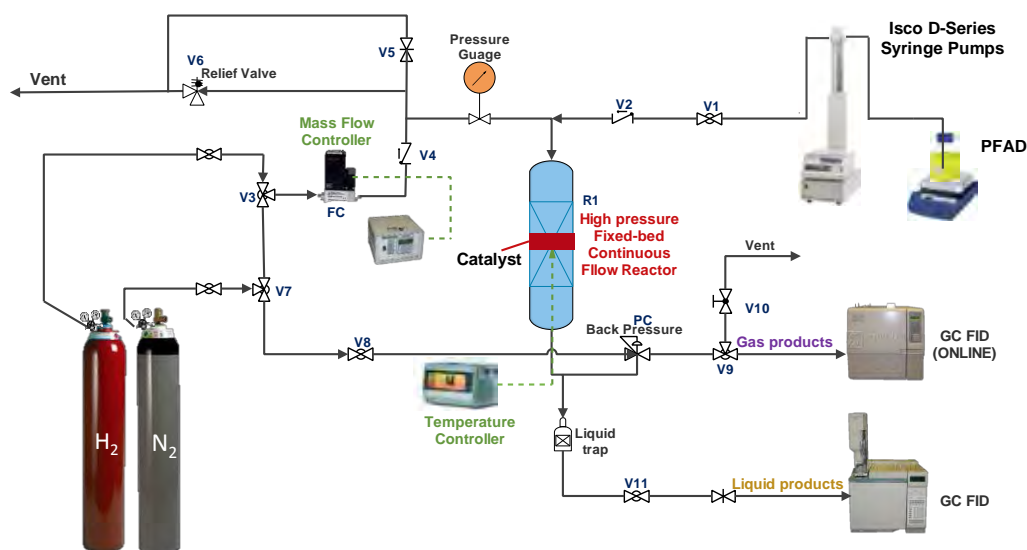


Figure 3.1 The schematic diagram of the reactor system.

Table 3.1 Description of system in flow diagram of the continuous flow fixed-bed reactor

No.	Part	Description
1	V1	On-off valve for feedstock from ISCO syringe pumps
2	V2	Checking valve for avoiding the backward flow of the feedstock
3	V3	Three ways valve for switching between nitrogen gas and hydrogen gas flow
4	V4	Checking valve for avoiding the backward flow of hydrogen or nitrogen gas
5	V5	Needle valve for releasing gas from the system
6	V6	Relief valve for releasing pressure overload in the system
7	V7	Three ways valve for switching the direction of nitrogen gas flow
8	V8	Needle valve for controlling pressure in back pressure regulator
9	V9	Three ways valve for switching between vent gas and gas to GC lines
10	V10	On-off valve for releasing pressure from back pressure regulator
11	V11	Metering valve for gathering the liquid product from condenser
12	R1	Continuous flow fixed-bed reactor where hydroprocessing reaction take place
13	FC	Flow controller to set flow rate for the desired H ₂ /feed molar ratio
14	PG	Pressure gauge for indicating pressure in packed bed reactor
15	PC	Back pressure regulator for controlling the pressure in reactor

The hydroprocessing reaction of palm oil is performed at temperature, pressure, liquid hourly space velocity (LHSV), and H₂/Feed ratio as shown in Table 3.2.

Table 3.2 The reaction conditions for hydroprocessing of palm fatty acid distillate in continuous flow fixed-bed reactor

Parameter	Value
Reaction Temperature (°C)	375-450
Reaction pressure (bar)	5, 10, 15, 30
LHSV (h ⁻¹)	1.5-2.5
Volume of Catalyst (ml)	4
H ₂ /feed molar ratio	10
Carrier gas	H ₂

3.5 Product Analysis

3.5.1 Liquid Products Analysis

The liquid products were quantified by a gas chromatograph (Agilent 7890) equipped with FID detector. The liquid products from the hydrocracking of hydrogenated biodiesel derived from palm oil contain non-polar hydrocarbons. The non-polar hydrocarbons were determined by using DB-5 column (non-polar column). The GC operating condition was summarized as follows:

Injector temperature:	50 °C
Detector temperature:	380 °C
Carrier gas:	He
Column type:	Capillary column (DB-5HT: diameter 0.32 mm length 30 m)

The following chromatographic temperature program in Table 3.3 was used for liquid product analysis:

Table 3.3 The chromatographic temperature program for liquid product analysis

Step	Temperature (°C)	Rate (°C/min)	Holding time (min)
1	50	-	5
2	169	10	10
3	380	20	10

For the quantitative calculations of liquid product, the areas of each peak analyzed hourly by a GC/FID (Agilent 7890) were converted to gram unit by Equation 3.1 because the each peak of products detected by FID detector can be varied from area unit to gram unit directly.

$$\text{Weight of product } i \text{ (g)} = \frac{(\text{areas of product } i) \times (\text{grams of liquid product})}{\text{total areas of liquid product}} \quad (3.1)$$

The conversion and products selectivity of each product were calculated by Equations 3.2 and 3.3:

$$\text{Conversion (\%)} = \frac{\text{moles of feed converted} \times 100}{\text{moles of feed input}} \quad (3.2)$$

$$\text{Selectivity to product } i \text{ (\%)} = \frac{\text{moles of product } i \times 100}{\text{moles of overall products}} \quad (3.3)$$

3.5.2 Gas Products Analysis

The composition of gas product was analyzed qualitatively on-line hourly by GC/FID (Shimadzu GC-17A). The GC operating condition was summarized as follows:

Injection temperature:	150 °C
Detector temperature:	250 °C
Carrier gas:	He
Column type:	capillary HP-PLOT/Al ₂ O ₃
	“S” deactivated column

The following chromatographic temperature program in Table 3.4 was used for gas product analysis:

Table 3.4 The chromatographic temperature program for gas-phase product analysis

Step	Temperature (°C)	Rate (°C/min)	Holding time (min)
1	40	-	3
2	70	15	0
3	170	5	0
4	190	1	1

For the quantitative calculations of gas product, the areas of each peak analyzed hourly by GC/FID (Shimadzu GC-17A) were converted to gram unit by comparing with the area of methane from gas standard by mol % (equal to vol %), as shown in Equations 3.4 .

$$\text{Weight of product } i \text{ (g)} = \frac{(\text{areas of product } i \text{ per 1 ml}) \times (\text{mol of methane per 1 ml}) \times (\text{overall gas product } (\frac{\text{ml}}{\text{h}}))}{(\text{mol of carbon atom}) \times (\text{reference area of methane per 1 ml}) \times (\text{molecular weight } i (\frac{\text{g}}{\text{mol}}))} \quad (3.4)$$

The calculations of conversion, selectivity and yield of product are defined as shown in Equations 3.5, 3.6 and 3.7, respectively.

$$\text{Conversion (\%)} = \frac{\text{weight of total products} \times 100}{\text{weight of feed input}} \quad (3.5)$$

$$\text{Selectivity of product } i \text{ (\%)} = \frac{\text{weight of product } i \times 100}{\text{weight of total products}} \quad (3.6)$$

$$\text{Yield of product } i \text{ (\%)} = (\text{conversion}) \times (\text{selectivity of product } i) \quad (3.7)$$

CHAPTER IV

RESULTS AND DISCUSSION

In this research, the catalysts were synthesized and investigated. There were Ni/HY, Pd/TiO₂, Ni/HY^{core}-Pd/TiO₂^{shell} catalysts prepared by incipient wetness impregnation, sol-gel, and Ni/HY^{core}-Pd/TiO₂^{shell} catalysts prepared by coating Pd/TiO₂ layer on core catalyst by single step sol-gel method respectively.

4.1 Characterization of Fresh Catalysts

In this work, the catalysts were synthesized and investigated. There were three parent catalysts includes Ni/HY, Pd/TiO₂; and Ni/HY^{core}-Pd/TiO₂^{shell} catalyst respectively.

4.1.1 X-ray Diffraction (XRD)

XRD patterns of synthesized Pd/TiO₂ (SG), Ni/HY^{core}-Pd/TiO₂^{shell} (SSSG), Ni/HY, and HY zeolite are shown in Figure 4.1. The characteristic peaks for core catalyst NiO species at $2\theta = 37.24^\circ$, 43.34° , and 64.48° , corresponding to the planes (111), (200), and (220) of cubic NiO species, respectively. Moreover, the characteristic peaks of Pd/TiO₂ catalyst illustrated the crystalline structure of the pure anatase phase due to the dominant peaks at $2\theta = 25.26^\circ$, 37.82° , 40.08° , 53.92° , 55.06° , 62.62° , 68.84° , 70.02° and 75.10° which represent the (101), (004), (200), (105), (211), (204), (116), (220) and (215) planes, respectively. In case of the core-shell catalysts, the xrd pattern showed a combined pattern of both Ni/HY and Pd/TiO₂ indicating that the prepared core-shell catalysts remained both of the parent structures.

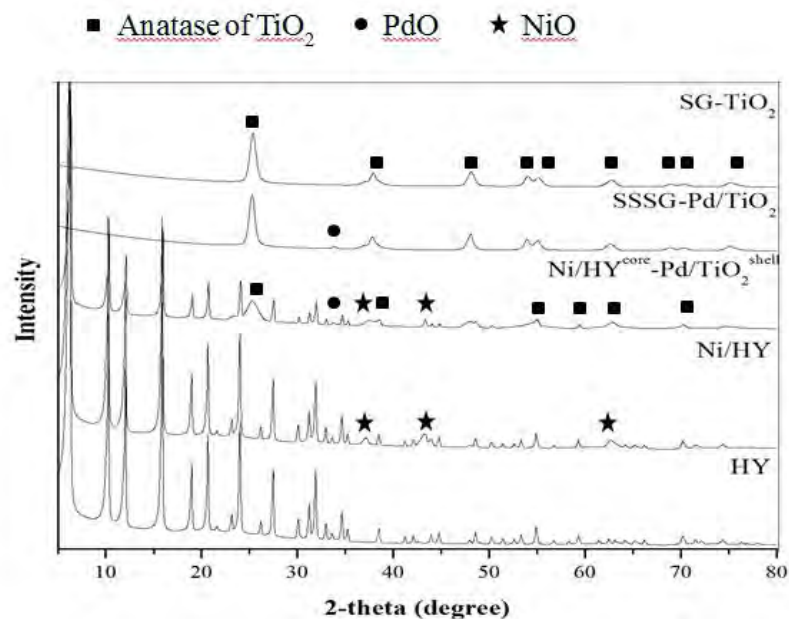


Figure 4.1 XRD patterns of synthesized parent HY, Ni/HY, Ni/HY^{core}-Pd/TiO₂^{shell}, and Pd/TiO₂ catalysts.

4.1.2 X-ray Photoelectron Spectroscopy (XPS)

X-ray photoelectron spectroscopy (XPS) was used to analyze oxidation state of palladium and nickel in the prepared catalysts. As can be seen in Figure 4.2, the peaks with binding energies of 337.2 and 341.8 eV were attributed to the Pd 3d_{5/2} and Pd 3d_{3/2} transitions, respectively (Karthikeyan *et al.* 2016). It was indicated the presence of palladium in the metallic state. Furthermore, the Figure 4.3 illustrates the Ni 2p_{3/2} XPS peaks were observed at 855.7, 861.2 eV and Ni 2p_{1/2} XPS peaks were observed at 879.5 and 873.6 eV, respectively. It indicated the presence of metallic nickel and NiO (Karthikeyan *et al.* 2016).

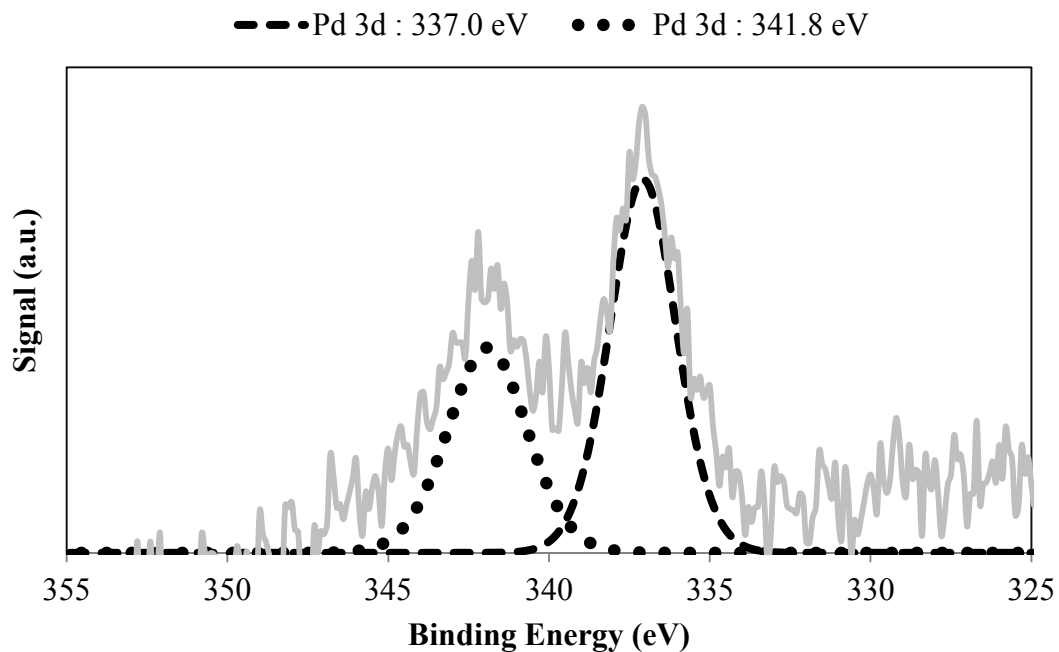


Figure 4.2 High resolution XPS spectrum of Pd 3d in Pd/TiO₂.

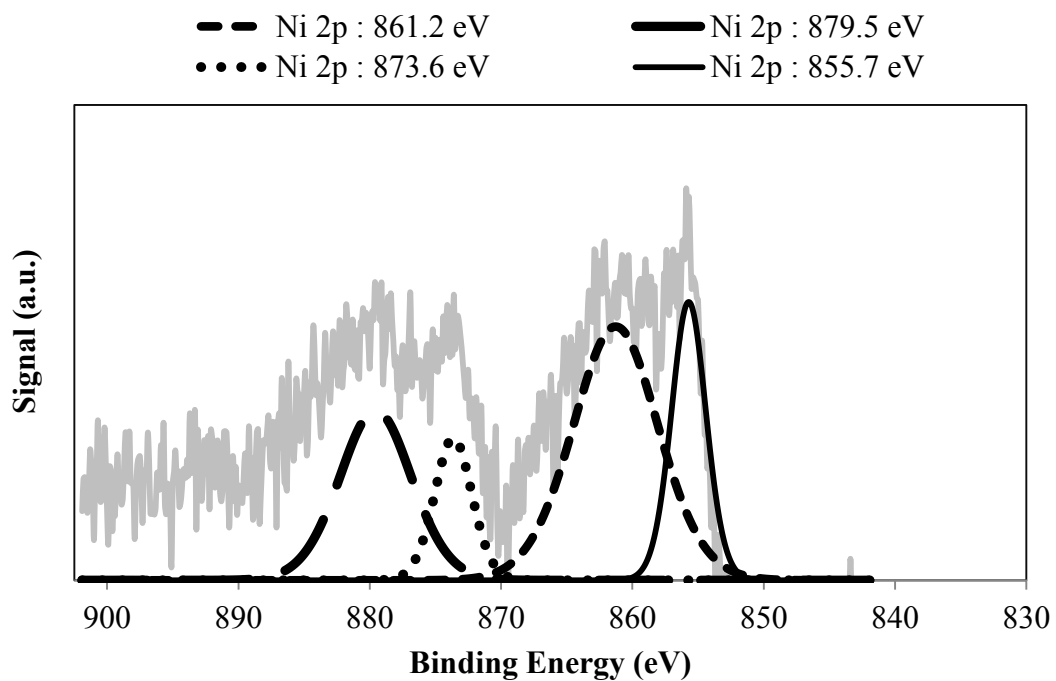


Figure 4.3 High resolution XPS spectrum of Ni 2p in Ni/HY.

4.1.3 Transmission Electron Microscope (TEM)

Transmission electron microscope (TEM) was used to identify the images of prepared catalysts. TEM images of Ni/HY catalyst are shown in Figure 4.4 (a) and (b). The dark spots in Figure 4.4 (b) were the nickel particles which highly dispersed on HY zeolite but their were some particle seem to be agglomerated due to impregnation method. The TEM images of core-shell catalyst can be explained that Ni/HY was covered with layer of Pd/TiO₂ catalyst.

From Figure 4.5 (a) and (b), the TEM images of Pd/TiO₂ exhibit higher dispersion of palladium metal in TiO₂ support due to single-step sol gel method. Moreover, it can be seen in Figure 4.5 (b) that 3.5 Å d spacing lattice fringes were represented the spacing of (101) planes of anatase, TiO₂ (Shen *et al.* 2008).

In Figure 4.6 (a) and (b), the TEM images illustrate of Ni/HY^{core}-Pd/TiO₂^{shell} catalyst at the outer area gave identical as Pd/TiO₂ catalyst while at the center with dark area represented of the Ni/HY catalyst. Therefore, core-shell structure can be confirmed.

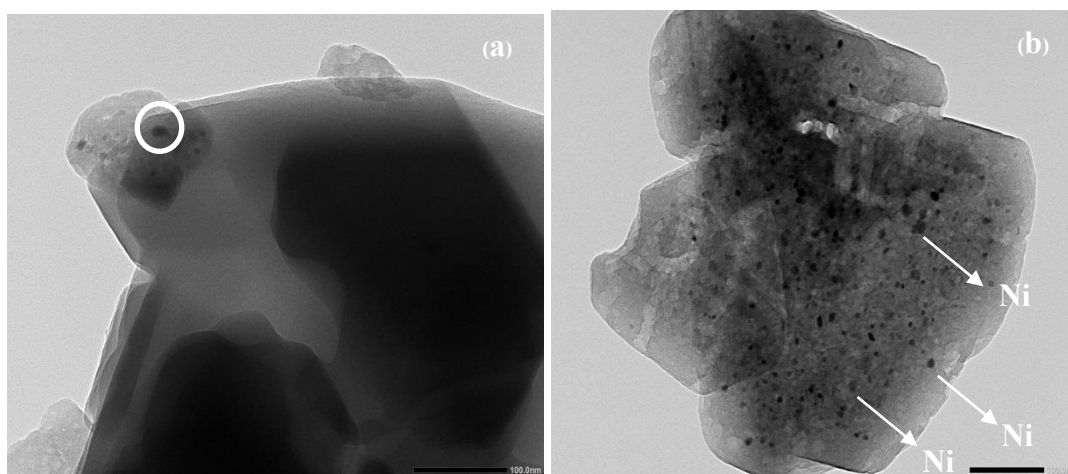


Figure 4.4 (a), (b) TEM images of Ni/HY core catalyst.

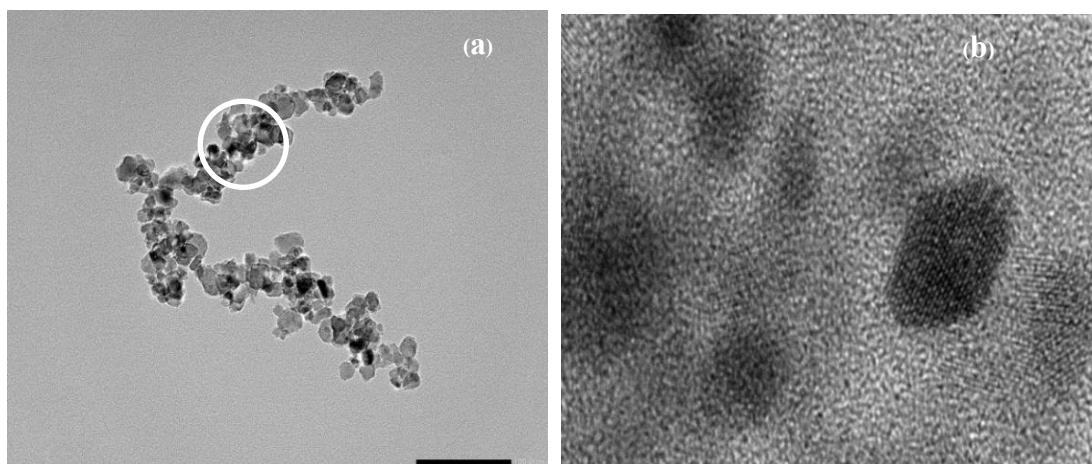


Figure 4.5 (a), (b) TEM images of Pd/TiO₂ shell catalyst.

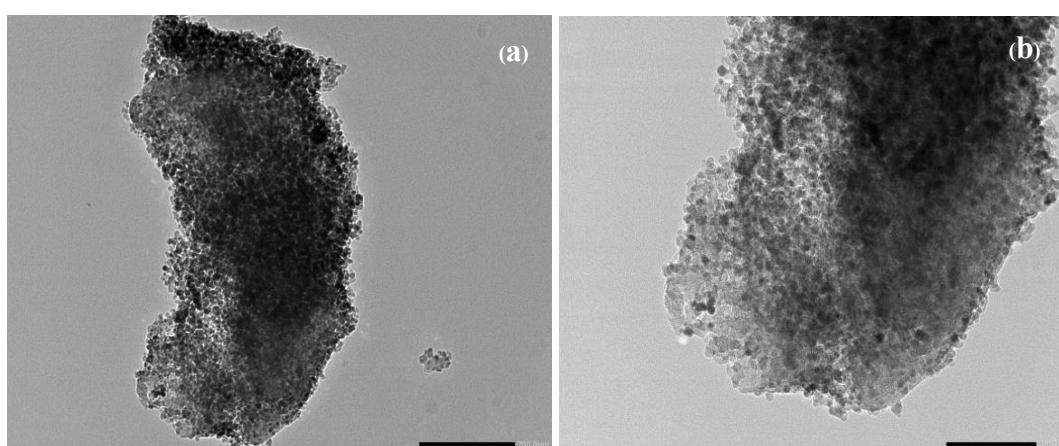


Figure 4.6 (a), (b) TEM images TEM images Ni/HY^{core}-Pd/TiO₂^{shell} catalyst.

4.1.4 Brunauer-Emmett-Teller (BET)

The surface area, pore size, and pore volume of the prepared catalysts are summarized in Table 4.1. The surface area of Ni/HY catalyst was higher than Pd/TiO₂ catalyst because microporous structure in Ni/HY catalyst and mesoporous structure in Pd/TiO₂ catalyst. In addition, the presence of Ni or Pd metal decreased the surface areas of both HY and TiO₂ support catalysts. The surface area and pore volume of Ni/HY^{core}-Pd/TiO₂^{shell} catalyst decreased gradually when Pd/TiO₂ content was introduced, corresponding to the characteristic of a mesoporous structure of Pd/TiO₂ catalyst.

Table 4.1 The textural properties of the prepared catalysts

Catalysts	Surface area (m ² /g)	Pore size (nm)	Pore volume (ml/g)
Ni/HY—Pd/TiO ₂	359	4.0	0.4
Pd/TiO ₂	69	8.8	0.2
TiO ₂	81	8.9	0.2
Ni/HY	535	3.3	0.4
HY	602	3.4	0.5

4.1.5 Temperature Programmed Desorption (TPD) of Isopropylamine

The Brønsted acid sites of prepared catalysts were quantified by using the temperature programmed desorption (TPD) of isopropylamine. The acid sites catalyze the conversion of isopropylamine into propylene and ammonia (Pereira and Gorte, 1992). Figure 4.7 demonstrates weak and strong Brønsted acid site peaks at 100 – 250 °C and 300 – 400 °C in both Ni/HY (core) and Ni/HY^{core}—Pd/TiO₂^{shell}, respectively. In addition, it can be observed that a small peak at 350 °C represented as a Brønsted acid sites of Pd/TiO₂. The Brønsted acidity of synthesized catalysts were summarized in Table 4.2, Ni/HY had the highest acidity which selective for cracking reaction. Moreover, it can be seen that the Brønsted acidities of Ni/HY^{core}—Pd/TiO₂^{shell} was decreased with TiO₂ contents and still contained the characteristic of parent catalysts.

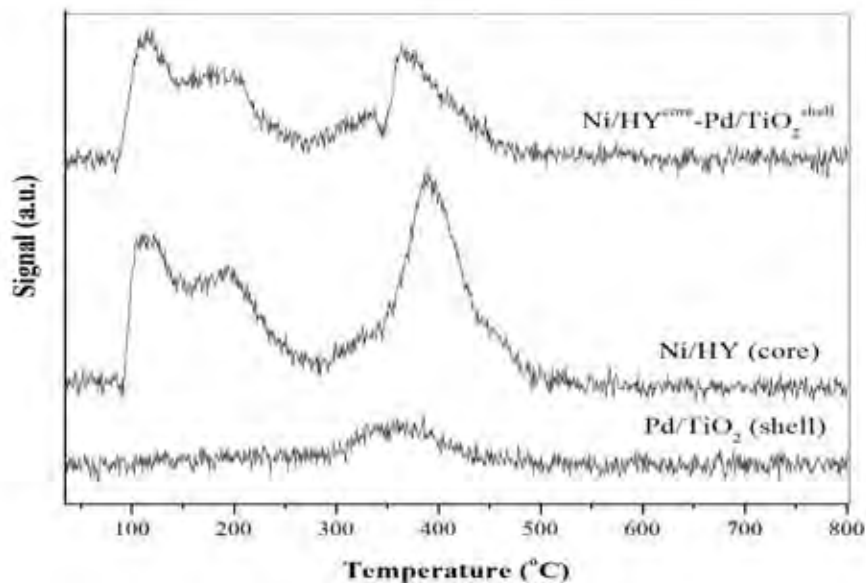


Figure 4.7 TPD profiles of prepared catalysts.

Table 4.2 Acidity of the prepared catalysts from TPD of isopropylamine

Catalysts	Brønsted Acidity (mmol/g)
Pd/TiO ₂ (shell)	0.5
Ni/HY (core)	3.3
Ni/HY ^{core} -Pd/TiO ₂ ^{shell}	2.1

4.1.6 Temperature Programmed Reduction (TPR)

Temperature programmed reduction was used to evaluate the reduction temperature of the prepared catalysts. The TPR profiles of both catalysts are presented in Figure 4.8. The presence of peak at 250-350 °C can be attributed to the reduction of NiO particles without the interaction with the support (Li *et al.*, 2010). According to the reported observations, at the temperature range of 350-650 °C was observed for the impregnated NiO-SiO₂ (Suzuki *et al.*, 1987). In addition, the reduction peak of Ni/HY at 550 °C is corresponding to the Ni in α -cage peaks according to Suzuki and co-workers. They found that the reducibility of the Ni²⁺ ions occupying sites SI (α cavity).

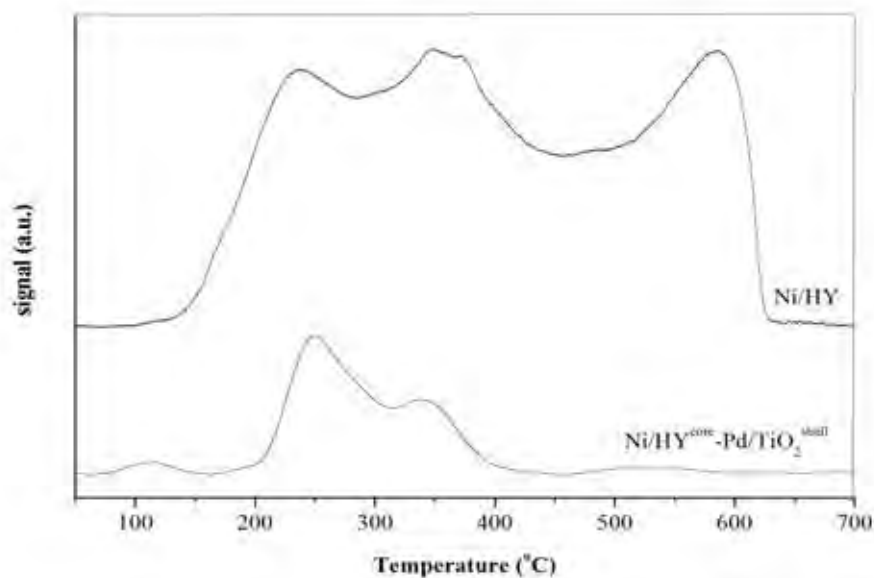


Figure 4.8 Temperature programmed reduction (TPR) profiles of the prepared Ni/HY and Ni/HY^{core}-Pd/TiO₂^{shell} catalysts.

4.2 Gas Chromatography of Feed and Standard Analysis

4.2.1 Feed Analysis

Figure 4.9 illustrates the chromatogram of various fatty acids components in feedstocks range including palmitic acid (22.0), oleic acid (27.6), stearic acid (28.2), mono-glycerides (32–33), di-glycerides (33–38) and tri-glycerides (38–43) analyzed by a GC/FID (Agilent 7890A). Besides, the composition of PFAD as shown in Table 4.3, it can be revealed that PFAD contains palmitic acid as main component and also trace amount of oleic acid, stearic acid, mono-, di- and tri-glycerides.

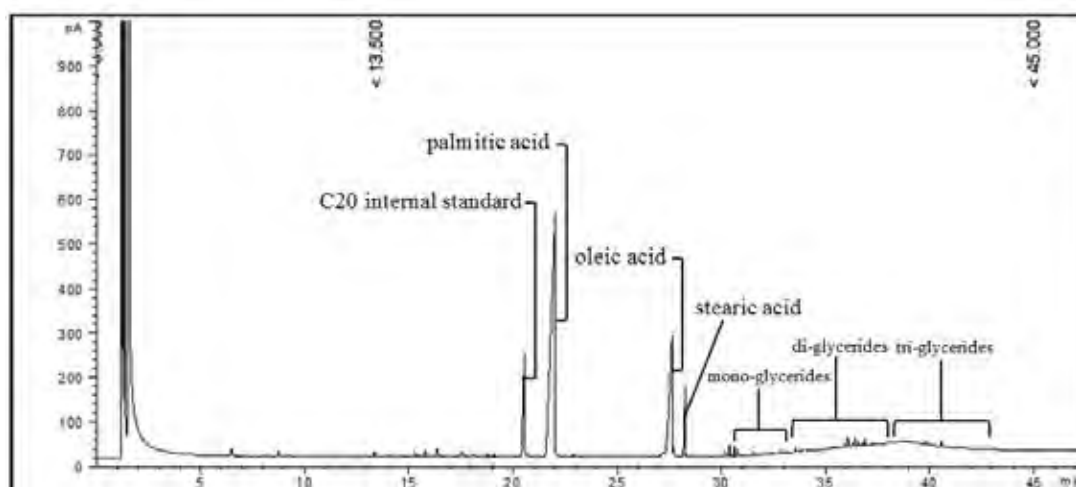


Figure 4.9 The chromatogram of various fatty acids components in PFAD range analyzed by a GC/FID.

Table 4.3 Composition of PFAD feedstock

Composition	PFAD (wt. %)
palmitic acid	92.10
oleic acid	3.61
stearic acid	0.33
mono-glycerides	0.90
di-glycerides	2.13
tri-glycerides	0.94

4.2.2 Standard Analysis

The chromatograms of liquid standard are analyzed by gas chromatograph equipped with an FID detector (Agilent 7890) to identify peaks of the compositions in feedstocks are shown in Figure 4.10 which are polarity liquid standard and Figure 4.11 which are non-polarity liquid standard.

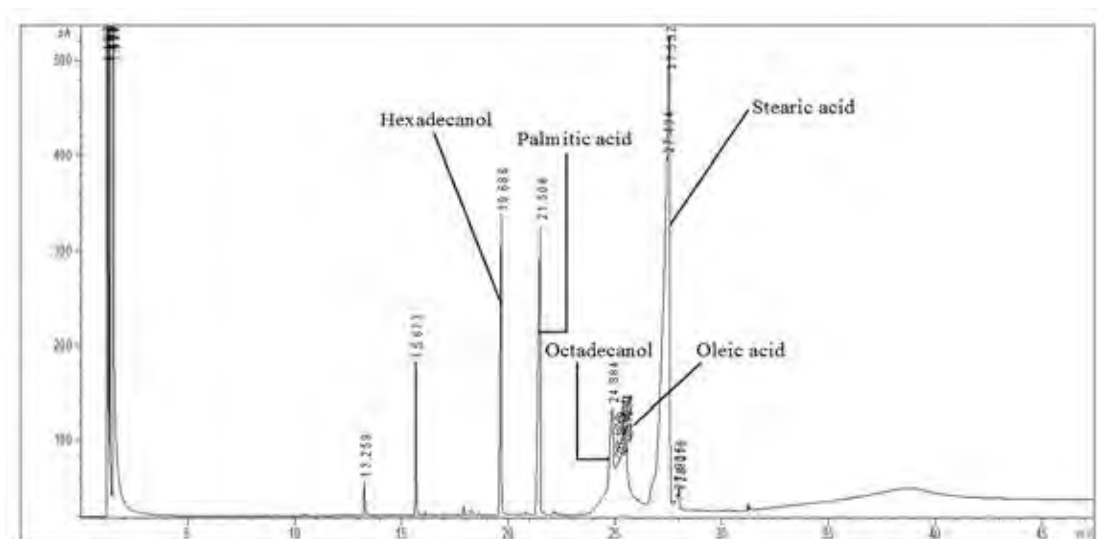


Figure 4.10 Chromatograms of standard oxygenated compounds.

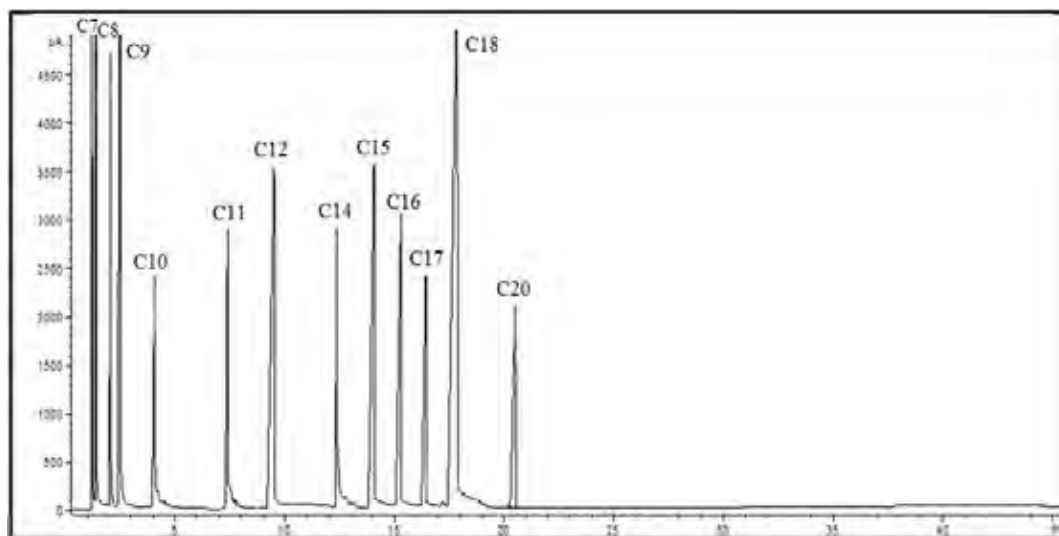


Figure 4.11 Chromatograms of standard *n*-alkanes.

Figure 4.10 shows the chemical standard of oxygenated compounds in types of fatty acid and alcohol which are feed and intermediates in catalytic activity testing. Moreover, the aliphatic hydrocarbons standards from catalytic activity testing such as heptane (C7), octane (C8), nonane (C9), decane (C10), undecane (C11),

dodecane (C12), tetradecane (C14), pentadecane (C15), hexadecane (C16), heptadecane (C17), and octadecane (C18) are also shown in Figure 4.9.

The chromatogram of liquid and gas products over Ni/HY^{core}-Pd/TiO₂^{shell} operated at operating conditions: 425 °C, 30 bar, LHSV of 1.5 h⁻¹, H₂/feed molar ratio of 10, and TOS of 6 h is shown in Figure 4.12, respectively. Palm fatty acid distillate on Figure 4.12 (a) is normally wax at room temperature and will be melting at 70 °C with dark brown colour. Moreover, the liquid products on Figure 4.12 (b) are clear with yellow colour and less viscous on all TOS. In Figure 4.12 (c), a chromatogram of liquid products were divided into three main parts which were gasoline fuel (C5-C8), jet fuel (C9-C14), diesel fuel (C15-C18), PFAD (palmitic acid, oleic acid, stearic acid), and oxygenates (fatty aldehyde, fatty alcohol, diglyceride, triglyceride) at the retention times of 1.37 – 1.80 min, 2.03 – 11.84 min, 13.23 – 16.69 min, 19.60 -24.90 min, 17.41 – 19.18 min and 25.00 – 39.00 min respectively. Finally, Figure 4.12 (d) reveals a chromatogram of gas products, consisting of light fuel (C1-C4) and gasoline fuel (C5-C8) at the retention times of 1.15 – 12.00 min and 12.50 – 24.00 min, respectively.

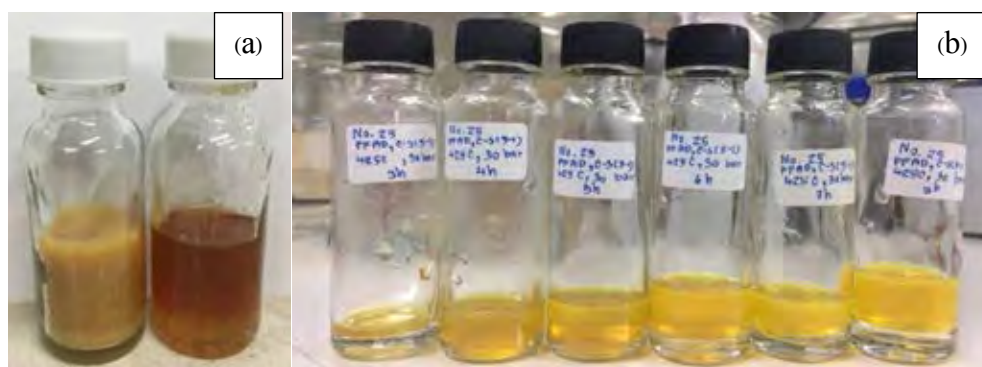


Figure 4.12 (a) Feed palm fatty acid distillate, (b) Liquid products, (c) liquid products chromatogram, and (d) gas products chromatogram obtained over Ni/HY^{core}-Pd/TiO₂^{shell} catalyst operated at operating conditions: 425 °C, 30 bar, LHSV of 1.5 h⁻¹, H₂/feed molar ratio of 10, and TOS of 6 h.

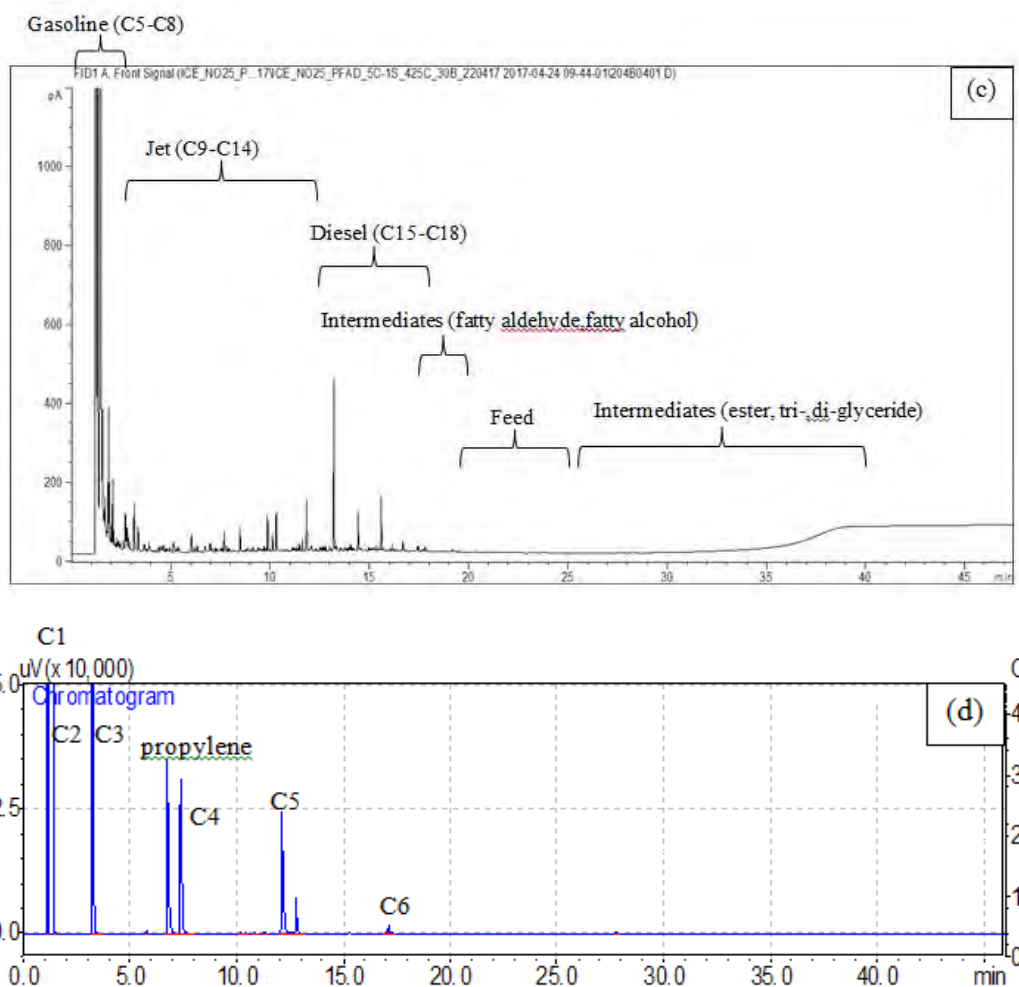


Figure 4.12 (Cont.) (a) Feed palm fatty acid distillate, (b) Liquid products, (c) liquid products chromatogram, and (d) gas products chromatogram obtained over $\text{Ni}/\text{HY}^{\text{core}}\text{-Pd}/\text{TiO}_2^{\text{shell}}$ catalyst operated at operating conditions: 425 °C, 30 bar, LHSV of 1.5 h^{-1} , H_2/feed molar ratio of 10, and TOS of 6 h.

4.3 Catalytic Activity Testing

In this part, the conversion, product yield and selectivity of from palm fatty acid distillate (fatty acid) over core-shell catalyst was investigated. The reaction conditions were conducted at temperature 375-450 °C, pressure 5-30 bar, liquid hourly space velocity (LHSV) of 1.5 h⁻¹, 2.0 h⁻¹ and 2.5 h⁻¹, and H₂/feed molar ratio of 10.

4.3.1 Effect of Core-shell Catalyst

Figure 4.13 exhibits the products selectivity from PFAD over the Ni/HY^{core}-Pd/TiO₂^{shell}, Ni/HY(core), and Pd/TiO₂(shell) catalysts at the same condition. The result indicated that selectivity of bio-jet fuel over core-shell catalyst was higher than selectivity of bio-jet fuel over Ni/HY(core) and Pd/TiO₂(shell) catalyst. The synthesized core-shell 5%Ni/HY^{core}-1%Pd/TiO₂^{shell} catalyst was reduced under H₂ at 450 °C for 3 h in order to activate the metal in active metal form.

The catalytic activity of 1%Pd/TiO₂ shell catalyst gave the lowest selectivity bio-jet fuel because shell catalyst selective for deoxygenation reaction. When the reaction occurred, PFAD was firstly converted to oxygenate compound which a large molecules can be blocked the active. In addition, Ni/HY (core) catalyst was selective for hydrocracking reaction due to the acidic properties of support. In addition, the core catalyst exhibited 100% conversion of PFAD into gasoline, jet, and diesel fuel range with very high *iso*-paraffin yield owing to hydrocracking and hydroisomerization reaction which are ordinary function of catalyst itself. Because of the molecule of fatty acid is too big to enter the micro pore in Ni/HY thus the feed need to be first crack on outer surface until the molecules can diffuse into the pore. In contrary, selective cracking will lead to high hydrocarbon production and lead to hydrocarbon blockage the pore without achieve the desire product. Furthermore, the modification core-shell catalyst exhibited highest bio-jet production of PFAD while decreasing of intermediates.

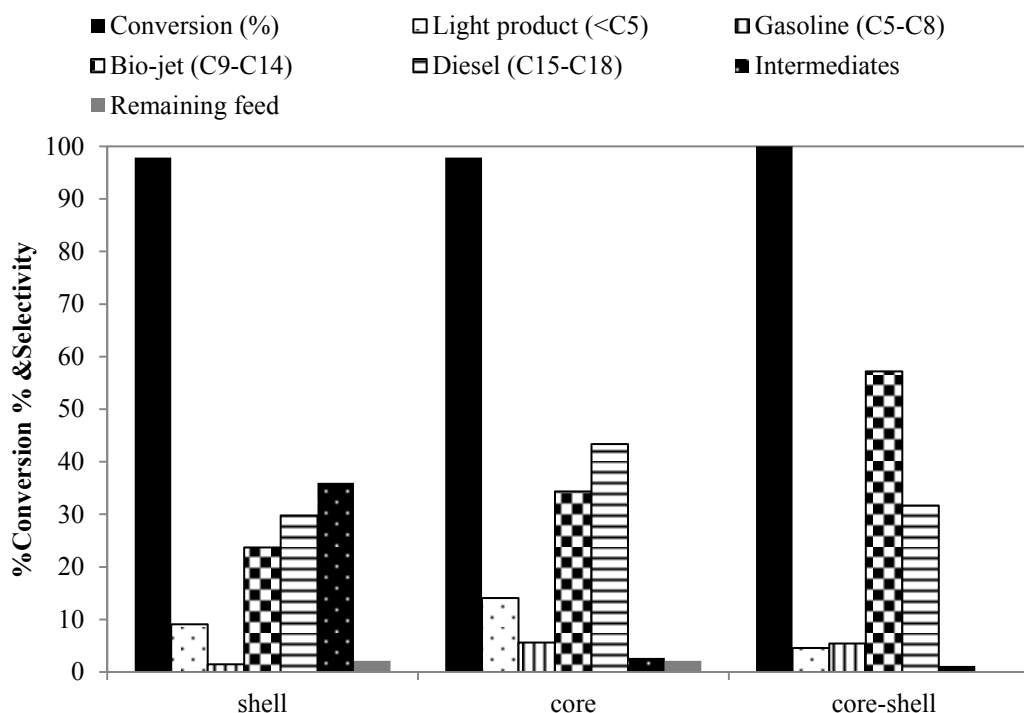


Figure 4.13 The conversion and selectivity of products that obtained over 1%Pd/TiO₂ shell, 5%Ni/HY core, and 5%Ni/HY^{core}-1%Pd/TiO₂^{shell} (Reaction condition: reaction temperature 425 °C, 30 bar, H₂/feed molar ratio of 10, LHSV of 1.5 h⁻¹, and TOS at 6 h).

The conversion and selectivity of Pd/TiO₂ catalyst is illustrated in Figure 4.14. It can be seen that at the first 3 h of the reaction diesel was obtained as the main product then declined dramatically by the next hour while trend of intermediates increased gradually with the function of time to become a major products. In addition, intermediates were observed during the catalytic activity testing because the deoxygenation of PFAD was occurred by transformation of PFAD into intermediates via hydrogenation (e.g. fatty aldehydes, fatty alcohols, fatty ester, and ketone) then further converted to long chain hydrocarbon like diesel (C15-C18) and jet (C9-C14) via decarbonylation.

Moreover, the products distribution is shown in Figure 4.15. It was observed large quantity of the main product was a long chain hydrocarbon (C9-C18). Due to feed composition, it was mainly belong to palmitic acid which is fatty acid

carbon atom 16, when the reaction took place at high temperature and high pressure not only decarboxylation/decarbonylation reaction can be occurred but the side reaction could be also obtained via hydrocracking and methanation reaction thus light hydrocarbon and methane were found with the presence of water and CO/CO₂, respectively. The overall hydrocarbon products can be seen in the Figure 4.15.

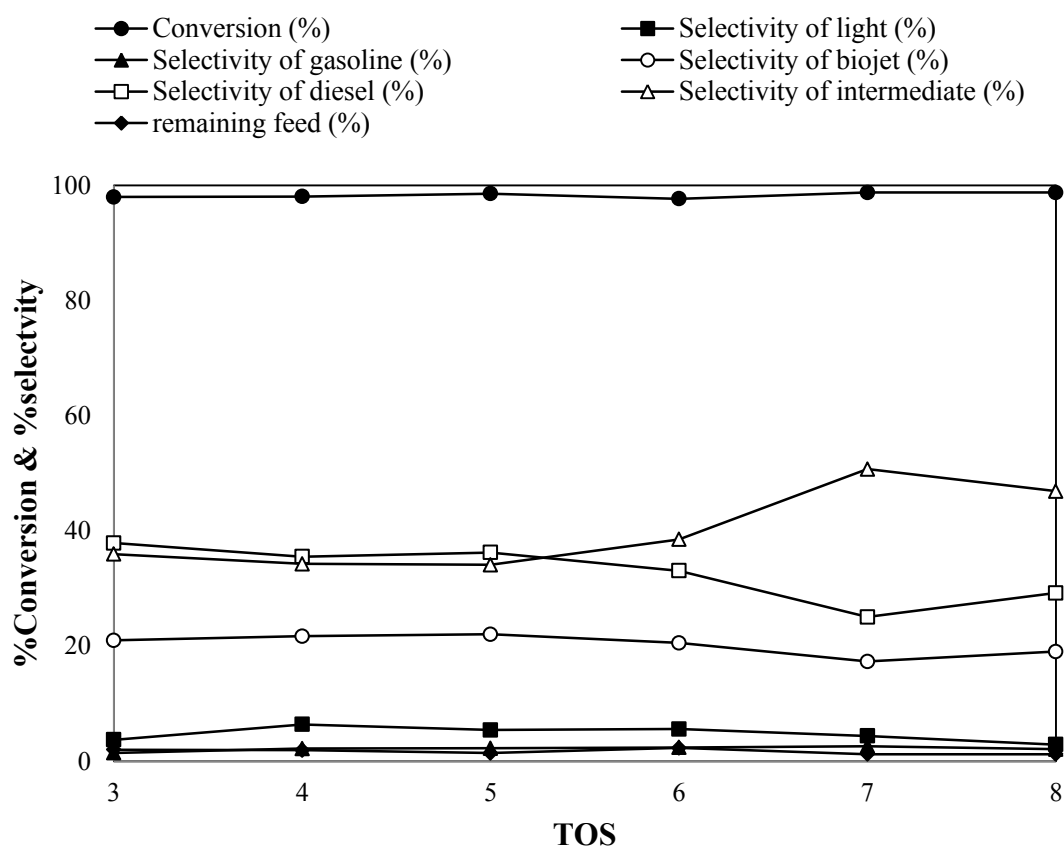


Figure 4.14 The conversion and selectivity of products that obtained over 1%Pd/TiO₂ (shell) at reaction condition: 425 °C, 30 bar, LHSV of 1.5 h⁻¹, and H₂/feed molar ratio of 10.

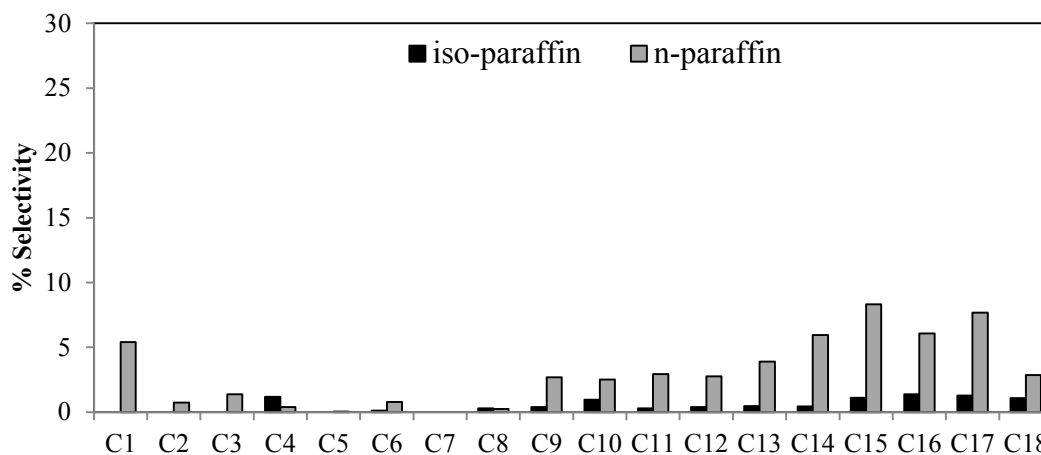


Figure 4.15 Product distribution of bio-jet production from PFAD over 1%Pd/TiO₂ (shell) catalyst at operating condition: 425 °C, 30 bar, LHSV of 1.5 h⁻¹, H₂/feed molar ratio of 10, and TOS of 6 h.

The catalytic activity of Ni/HY (core) can be seen in Figure 4.16. The carboxylic group can be eliminated via hydrodeoxygenation, or direct cracking of fatty acid molecules due to the severe condition. Hence, at the first period biojet (C9-C14) were observed as a main product and decreased slightly over time. In the contrary, diesel was increased sharply with time. It can be described by at the first hour of the reaction took place, diesel was converted very rapidly into smaller molecules such as jet, gasoline, and lighter because it was a severe condition with high temperature and pressure however over the time the water or the large molecules could be block the pore hence long chain hydrocarbons cannot be able to enter to Ni/HY and mainly diesel (C15-C18) was found as main products at later hour.

Furthermore, it can be seen in Figure 4.17 that *iso*-paraffin products were obtained in Ni/HY because the Brønsted acid site provides in HY catalyst generate the carbocation had influence on the isomerization reaction. In addition, when feed was fed into the system and adsorbed then cracked on the outer surface of the catalyst to remove oxygenate compound as CO, CO₂, and H₂O via reaction that explained above and further cracked to carbon atom 8 then cracked to carbon atom 4 as a series which *n*-paraffin hydrocarbons. Moreover, consisting of water in the system contribute to the competitive adsorption between the hydrocarbon

intermediates and water during the reaction. Consequently, active sites were blocked thus lowering the reaction activity.

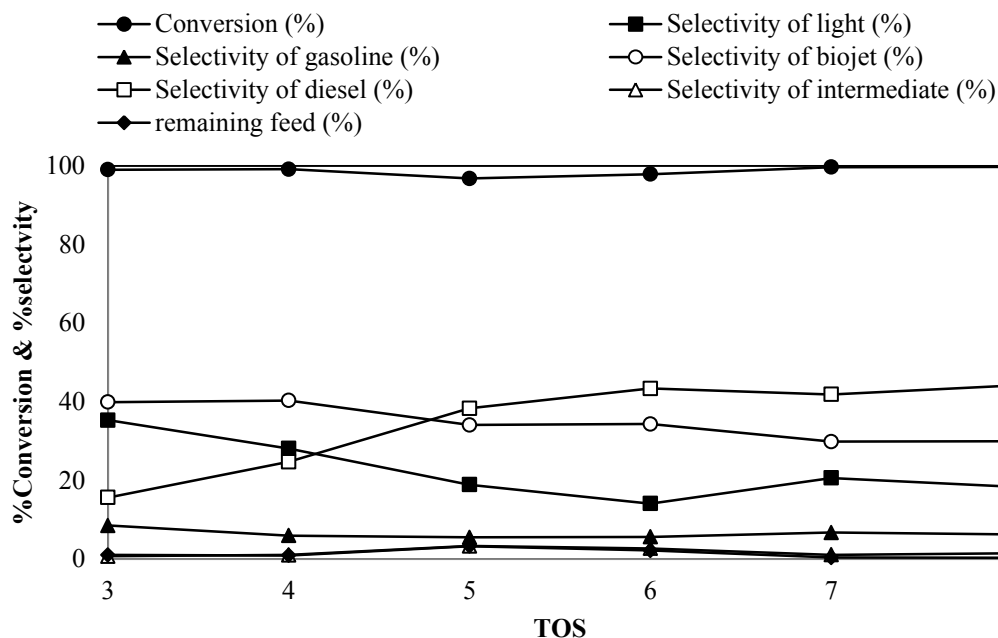


Figure 4.16 The conversion and selectivity of products that obtained over 5% Ni/HY (core) at reaction condition: 425 °C, 30 bar, LHSV of 1.5 h⁻¹, and H₂/feed molar ratio of 10.

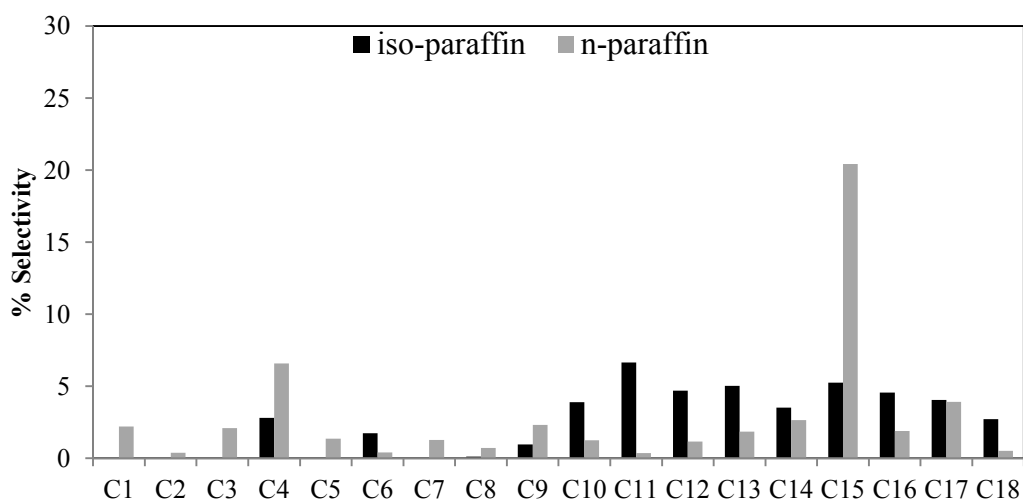


Figure 4.17 Product distribution of bio-jet production from PFAD over 5%Ni/HY (core) catalyst at operating condition: 425 °C, 30 bar, LHSV of 1.5 h⁻¹, H₂/feed molar ratio of 10 and TOS of 6 h.

The conversion and product selectivity over 5%Ni/HY^{core}-1%Pd/TiO₂^{shell} is illustrated in Figure 4.18. It can be seen that the selectivity of liquid bio-jet fuel slightly increased over time on stream until 6 h. Afterwards, the bio-jet production was gradually decreased with increasing of diesel and intermediates with time. This is because an intermediate should be converted into long chain hydrocarbons however it might be large molecules deposit on the porous surface hence bulking active site of cracking reaction. Moreover, Figure 4.19 shows *n*-paraffin and *iso*-paraffin yield from one-pot reaction of PFAD over core-shell catalyst which provides higher bio-jet fuel, lower intermediates, and lighter products than Ni/HY (core) and Pd/TiO₂ (shell) catalysts. It can be explained that core-shell catalyst play in the role with the deoxygenation then subsequently hydrocracking/isomerization reaction as one time by Pd/TiO₂ had responsibility to eliminate -COOH group from PFAD thus long chain hydrocarbon was obtained and further transported into the pore of Ni/HY for cracking/isomerization to shorter chain hydrocarbons, respectively.

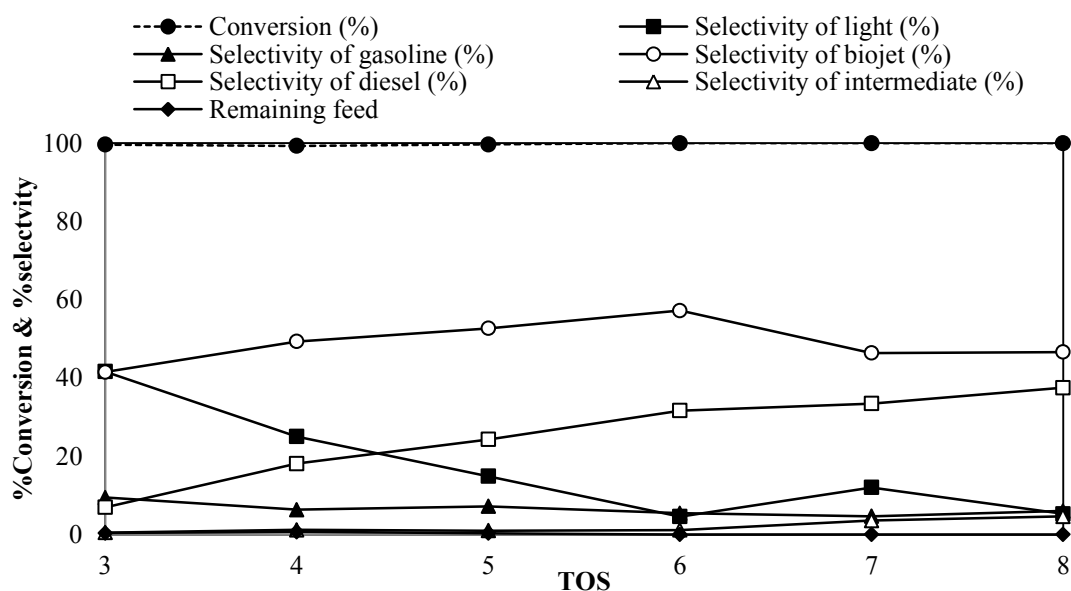


Figure 4.18 The conversion and selectivity of products that obtained over 5%Ni/HY^{core}-1%Pd/TiO₂^{shell} at reaction condition: 425 °C, 30 bar, LHSV of 1.5 h⁻¹, and H₂/feed molar ratio of 10.

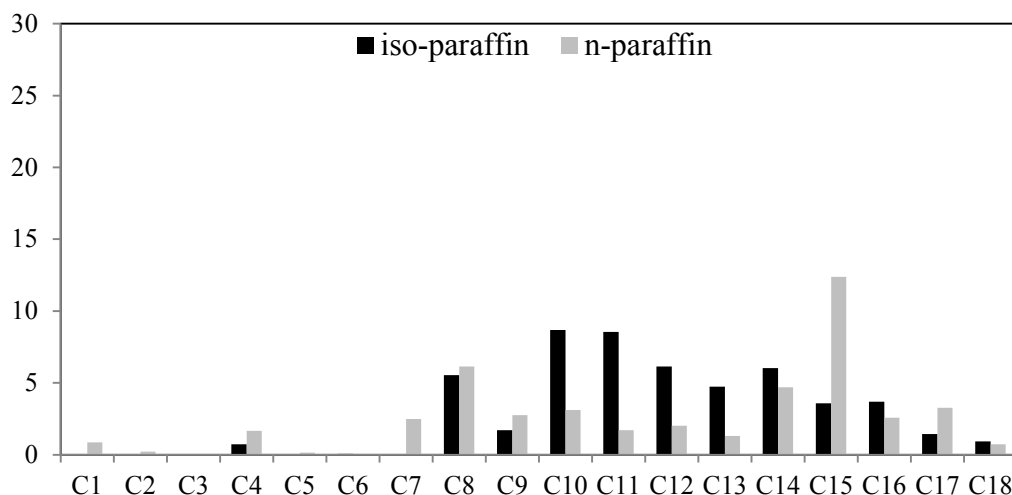


Figure 4.19 Product distribution of bio-jet production from PFAD over 5%Ni/HY^{core}-1%Pd/TiO₂^{shell} catalyst at operating condition: 425 °C, 30 bar, LHSV of 1.5 h⁻¹, H₂/feed molar ratio of 10, and TOS of 6 h.

4.3.2 Effect of Reaction Temperature

In order to study the effect of reaction temperature on product selectivity, the biojet production from PFAD was conducted at 5 bar, LHSV of 1.5 h⁻¹, and H₂/feed molar ratio of 10. The reaction temperature was varied from 375 to 450 °C. Figure 4.20 shows the effect of reaction temperature at 5 bar, the results demonstrated that at lower reaction temperatures the selectivity towards to hydrocarbons in the range of biojet was decreased. In addition, at reaction temperature 375 °C exhibited the highest selectivity of diesel (C15-C18) and intermediates which were fatty aldehyde and fatty alcohol influence ester wax blockage the pore inhibited hydrocracking reaction to the desire product. In contrary, the formation of intermediates can be decreased by increasing temperature up to 450 °C. Figure 4.21 can be explained that hydrocarbons in the range of jet (C9-C14) which were main component in biojet increased with increasing reaction temperature. In addition, hydrocracking to biojet and lighter hydrocarbon products was favor at higher temperature. This indicated that higher reaction temperature gave higher cracking product. Therefore, the reaction temperature at 425 °C was selected

as reaction temperature for further study the biojet production due to lowering intermediate and moderate amount in lighter gas (C1-C4) production.

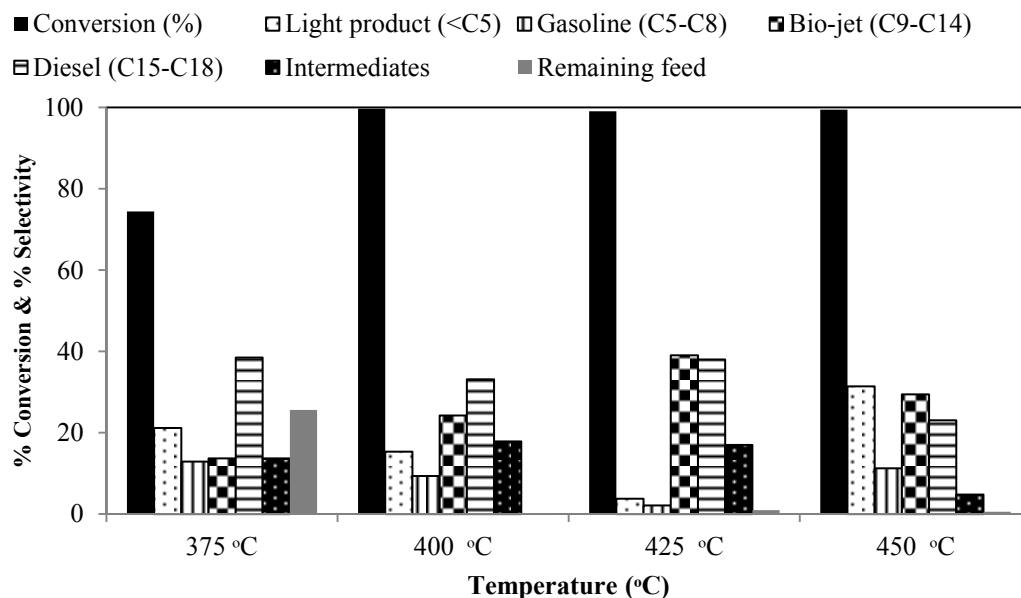


Figure 4.20 The conversion and selectivity of products that obtained over 5%Ni/HY^{core}-1%Pd/TiO₂^{shell} at different temperature (Reaction condition: 5 bar, H₂/feed molar ratio of 10, LHSV of 1.5 h⁻¹, and TOS at 6h).

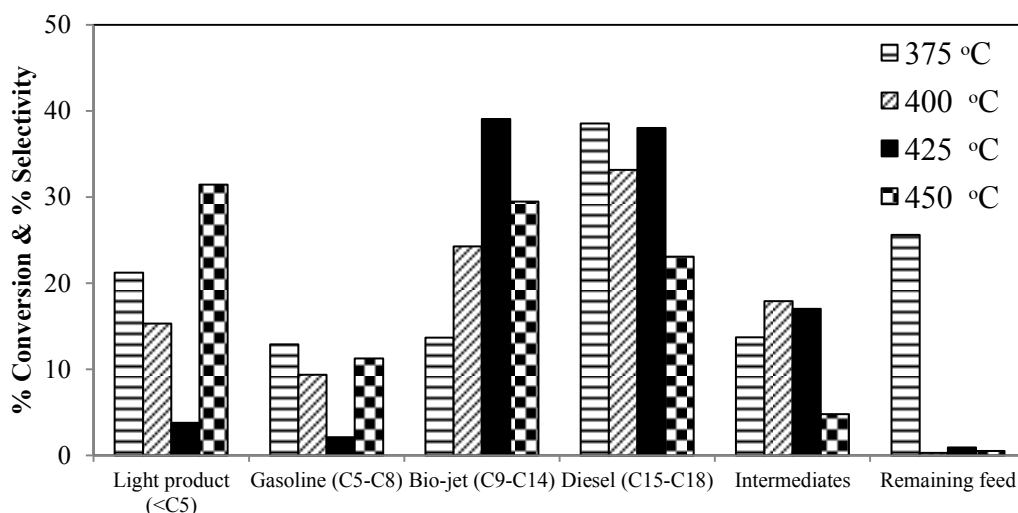


Figure 4.21 The product distribution over 5%Ni/HY^{core}-1%Pd/TiO₂^{shell} at different temperature (Reaction condition: 5 bar, H₂/feed molar ratio of 10, LHSV of 1.5 h⁻¹, and TOS at 6h).

4.3.3 Effect of Reaction Pressure

In order to study the effect of reaction temperature on product selectivity, the bio-jet production from PFAD was conducted at 425 °C, LHSV of 1.5 h⁻¹, and H₂/feed molar ratio of 10. The pressure was varied from 5 to 30 bar. Figure 4.22 illustrates the effect of increasing H₂ pressure from 5 up to 30 bar at reaction temperature of 425 °C. It can be found that increasing pressure results in increasing of hydrocarbons in the range of bio-jet fuel. Moreover, it can be observed that intermediates were decreased from 17.01% to 1.14% at high pressure level because intermediates (such as fatty aldehyde, fatty alcohol, and ester) can be more converted to biojet fuel products from 19.48% to 48.53%, respectively.

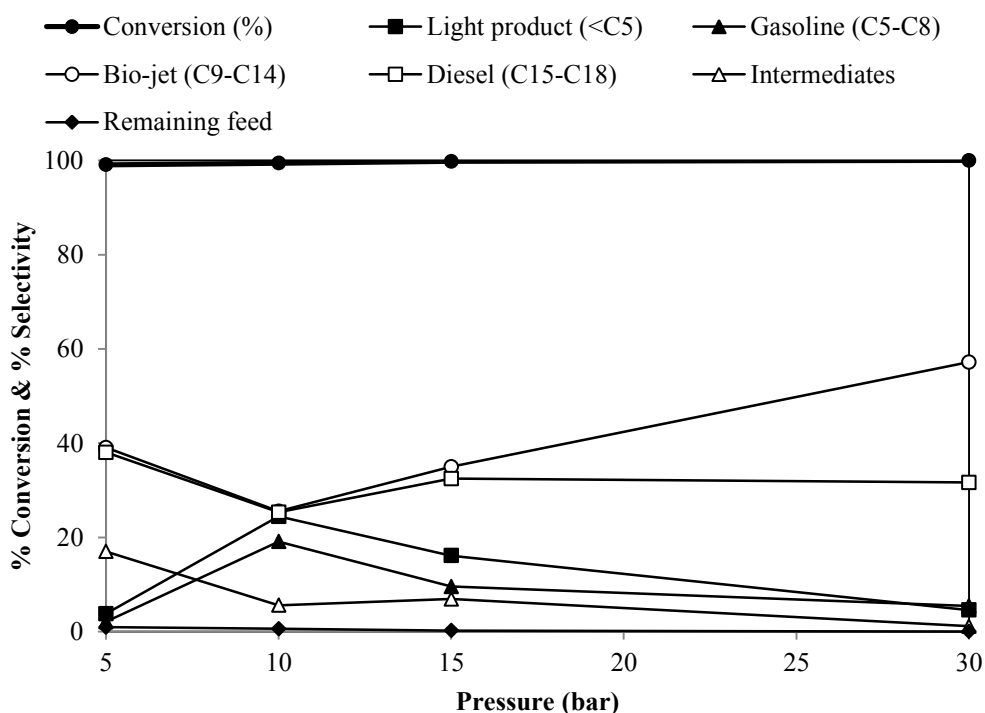


Figure 4.22 The conversion and selectivity of products that obtained over 5%Ni/HY^{core}-1%Pd/TiO₂^{shell} at different pressure (Reaction condition: reaction temperature at 425 °C, H₂/feed molar ratio of 10, LHSV of 1.5 h⁻¹, and TOS at 6h).

4.3.4 Effect of LHSV_s

The effect of LHSV_s on the products selectivity was also studied at operating condition: 425 °C, 30 bar, H₂/feed molar ratio of 10, TOS of 6 h and LHSV of 1.5, 2.0 and 2.5 h⁻¹. An increase of the liquid hourly space velocity (LHSV) did not influence the formation of bio-jet. From Figure 4.23, it can be observed that when LHSV increased from 1.5 h⁻¹ to 2.0 h⁻¹, it decreased activity of hydrocracking/hydroisomerization reaction results in the decline of bio-jet (C9-C14), gasoline (C5-C8), and lighter products while forming an intermediate (fatty aldehyde, fatty alcohol, and ester). Due to the shorter residence time of increasing LHSV, as all PFAD was converted, the existing aldehyde to alcohol intermediates which a large molecule was strongly adsorb on the active site lead to heavier hydrocarbon range and less cracking to produce hydrocarbon in the range of jet.

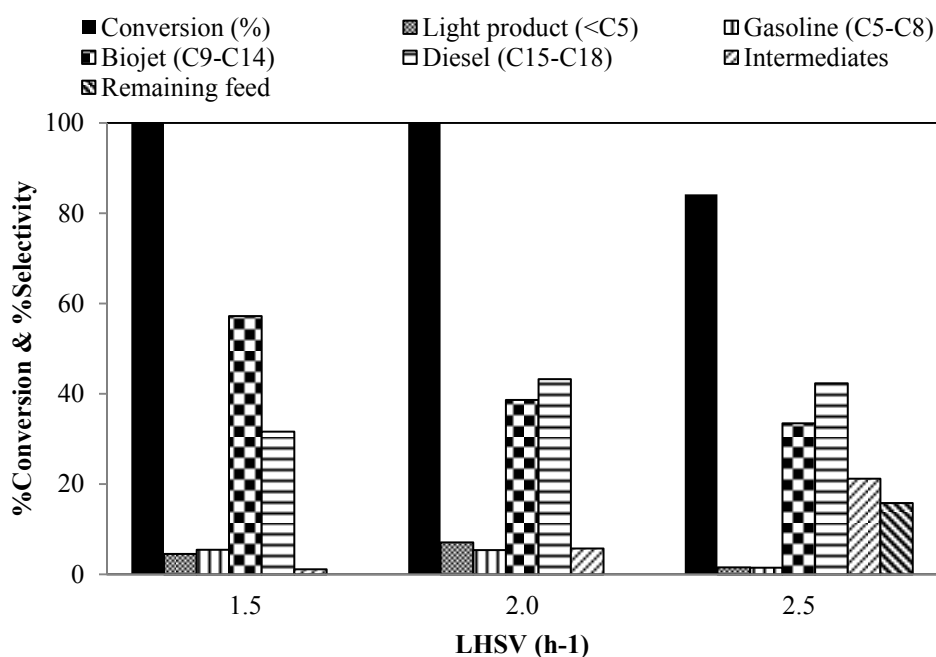


Figure 4.23 The conversion and selectivity of products that obtained over 5%Ni/HY^{core}-1%Pd/TiO₂^{shell} at different LHSV (Reaction condition: reaction temperature at 425 °C, 5 bar, H₂/feed molar ratio of 10, and TOS at 6 h).

4.4 Reaction Pathway

From Figure 4.24, it can be concluded that catalytic reaction of PFAD to biojet fuel over Pd/TiO₂. Palmitic acid could be direct decarboxylated to *n*-alkane and also obtained CO₂ as a by-product or the direct decarbonylation of fatty acid, via hydrogenated fatty acid to form fatty aldehyde intermediate which can be further decarbonylation to long chain hydrocarbons (i). In the contrary, fatty aldehyde intermediate can be hydrogenated to form fatty alcohol which goes through decarbonylation to produce long chain hydrocarbons. Moreover, fatty ester intermediates was formed by esterification over Lewis acid sites, it can also be converted to long chain hydrocarbon hydrogenolysis over metallic sites (ii). Feed can be adsorbed on oxygen vacancies defect sites in parallel to form carboxylates, the α -hydrogen was subsequently abstracted on the surface of catalyst to form ketene. The ketene intermediates can have an interaction with the neighboring carboxylate (palmitate) over TiO₂ support and form ketone (palmitone) by elimination of CO₂ (iii). If in the presence of hydrogen, ketene was further converted to large hydrocarbon molecules via aldehyde/alcohol intermediate over Pd metal sites through decarbonylation pathway. From Figures 4.25 and 4.26, it can be seen that the most intermediates were 1-hexadecanol from the reaction over Pd/TiO₂ was favored the direct decarboxylation/decarbonylation pathway.

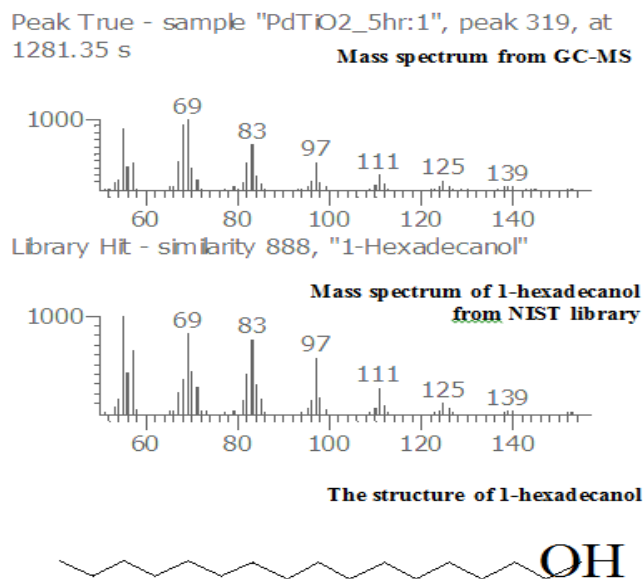


Figure 4.26 The mass spectrum of wax that obtained from GC/MS of 1-hexadecanol from NIST Library.

Figure 4.27 illustrates the catalytic reaction pathway over Ni/HY. Because Brønsted acid sites favor dehydration reaction, the sequential hydrogenation-dehydration-hydration route (hydrodeoxygenation reaction) was predominant in this catalyst. For those reasons, fatty aldehyde and alcohol were main intermediates to produce long chain hydrocarbons. The ability of the Ni metallic sites was selective for decarbonylation reaction. In addition, the abundance Brønsted acid sites in zeolite HY performed in row of isomerization reaction to produce *iso*-paraffin. From Figure 4.28, it can be seen that main intermediates were from by hydrogenation-dehydration reaction.

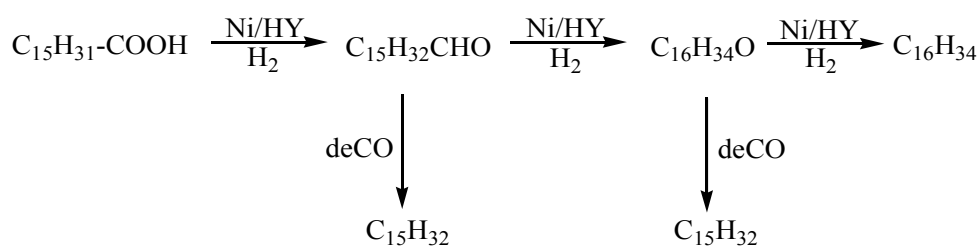


Figure 4.27 Proposed reaction pathway of biojet production from PFAD over Ni/HY.

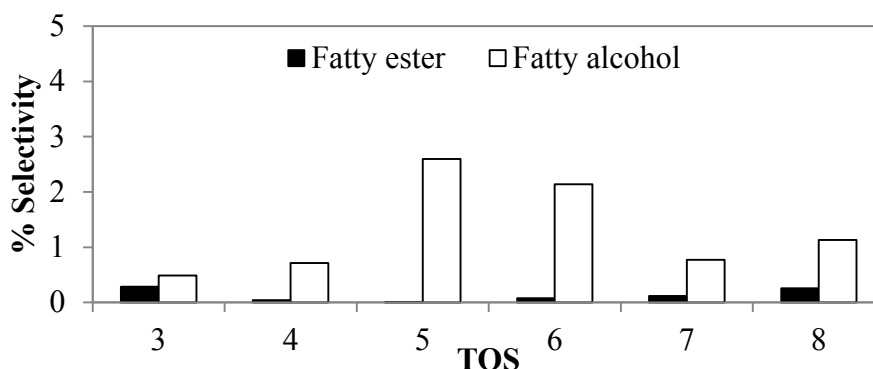


Figure 4.28 Selectivity of intermediates from biojet fuel production over Ni/HY at reaction condition: 425 °C, 30 bar, LHSV of 1.5 h⁻¹, and H₂/feed molar ratio of 10.

Summarized reaction pathway can be seen in Figure 4.29. The proposed pathway of bio-jet production from PFAD was deoxygenation of fatty acid to long chain hydrocarbon then further hydrocracking/hydroisomerization. There are three major reaction pathways to convert deoxygenation fatty acid to long chain hydrocarbon by (i) HDO pathway which consumed large quantity of H₂ and consequences produce H₂O, fatty acid was transformed to aldehyde as an intermediate then subsequently converted to alcohol and further cracking and isomerization to desire product, (ii) DeCO pathway, fatty acid can be transformed by eliminated carbonyl group as CO, (iii) DeCO₂ pathway, occur by elimination -COOH as CO₂ which consumed no H₂ and favor increasing reaction temperature.

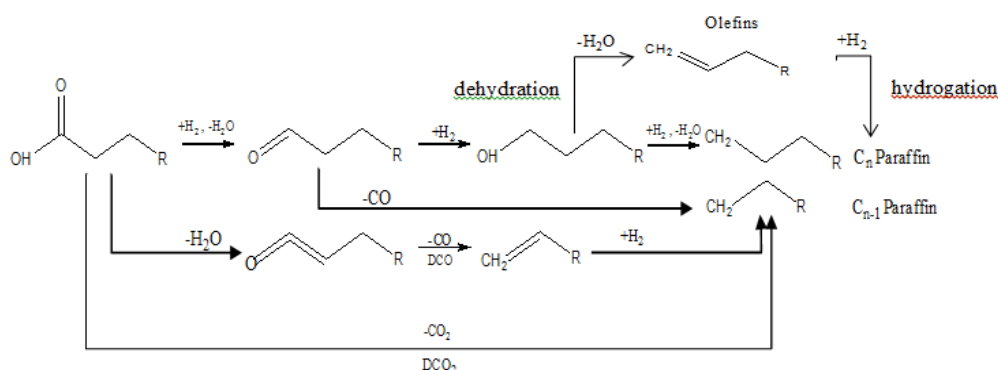


Figure 4.29 Proposed reaction pathways of deoxygenation of fatty acid.

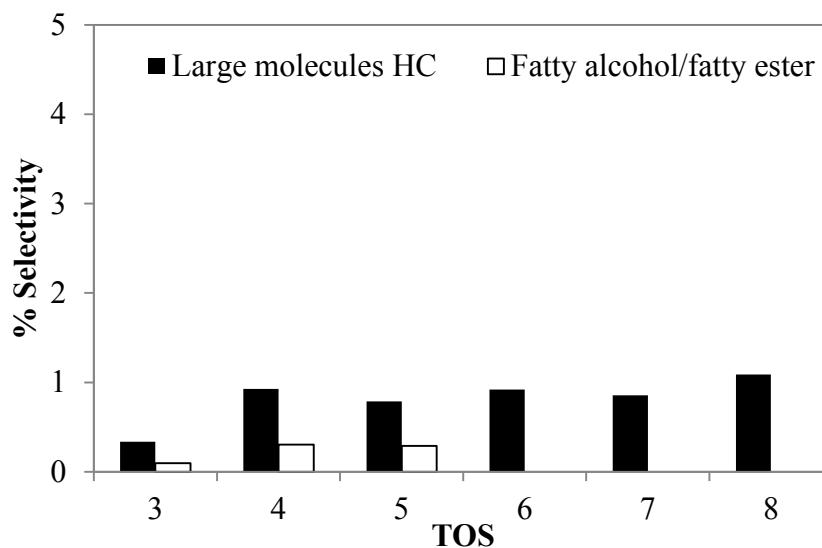


Figure 4.30 Selectivity of intermediates from biojet fuel production over 5%Ni/HY^{core}-1%Pd/TiO₂^{shell} at reaction condition: 425 °C, 30 bar, LHSV of 1.5 h⁻¹, and H₂/feed molar ratio of 10.

From Figure 4.18, as observed that conversion of PFAD was reached up to 100% along with time on stream (except in the first and second hour which are not stable system). As time was increased from third hour, bio-jet was slightly decreased while intermediate was increasingly observed. This can be clarified by, the first working reaction was deoxygenation from palm fatty acid distillate into long chain hydrocarbon in the range of diesel (C15–C18) then further did the hydrocracking process (Figure 4.31 (c) and Figure 4.32 (c)) into bio-jet range (C9–C14) was gradually dropped because bulking large molecule in HY pores. On the contrary, the diesel product and intermediates were increased at the end of the activity testing. Figure 4.30 shows the intermediates that appeared in this reaction, the intermediates were more selective to decarboxylation/decarbonylation reaction by the function of Pd/TiO₂ catalyst. Moreover, the Lewis acid sites that generated by oxygen vacancies can also be provided fatty esters which can do the hydrogenolysis to large hydrocarbon molecule. Thus these kinds of intermediate can be one case for deactivation.

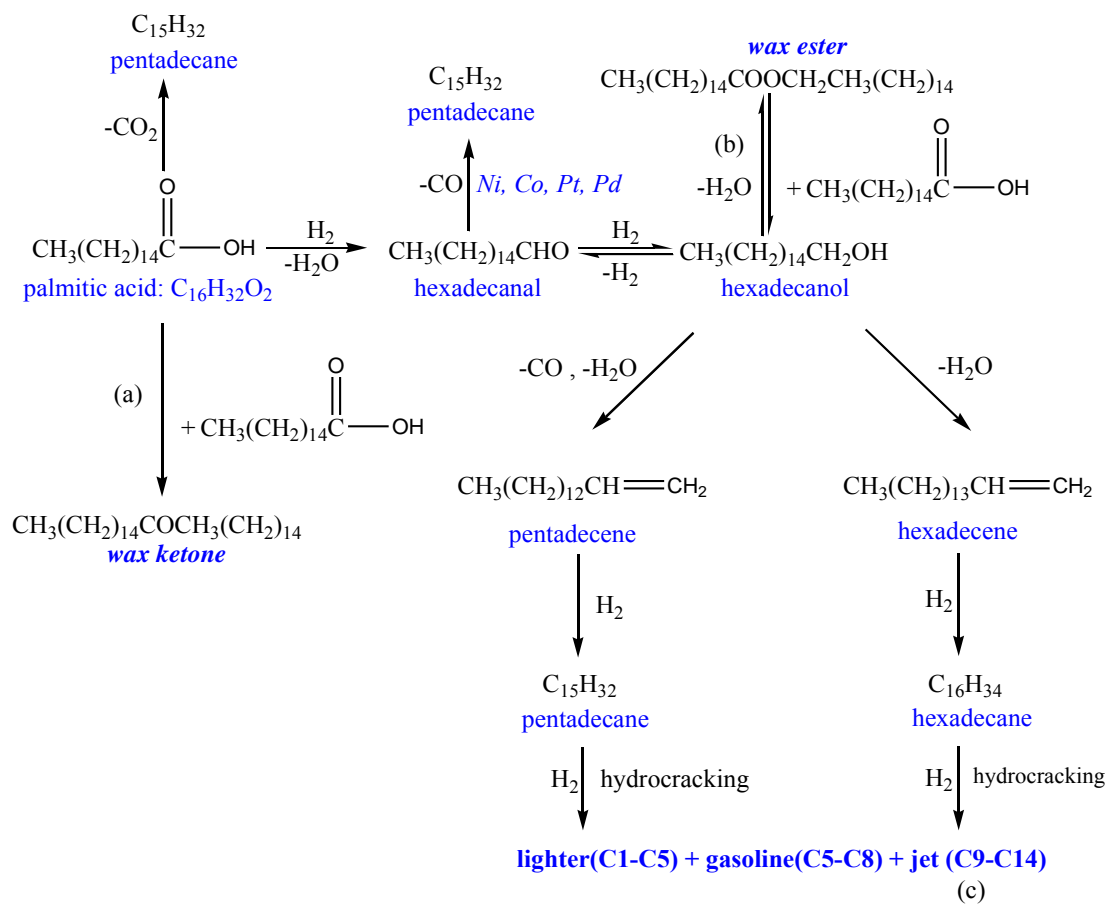


Figure 4.31 Proposed reaction pathway of palmitic acid to hydrocarbons.

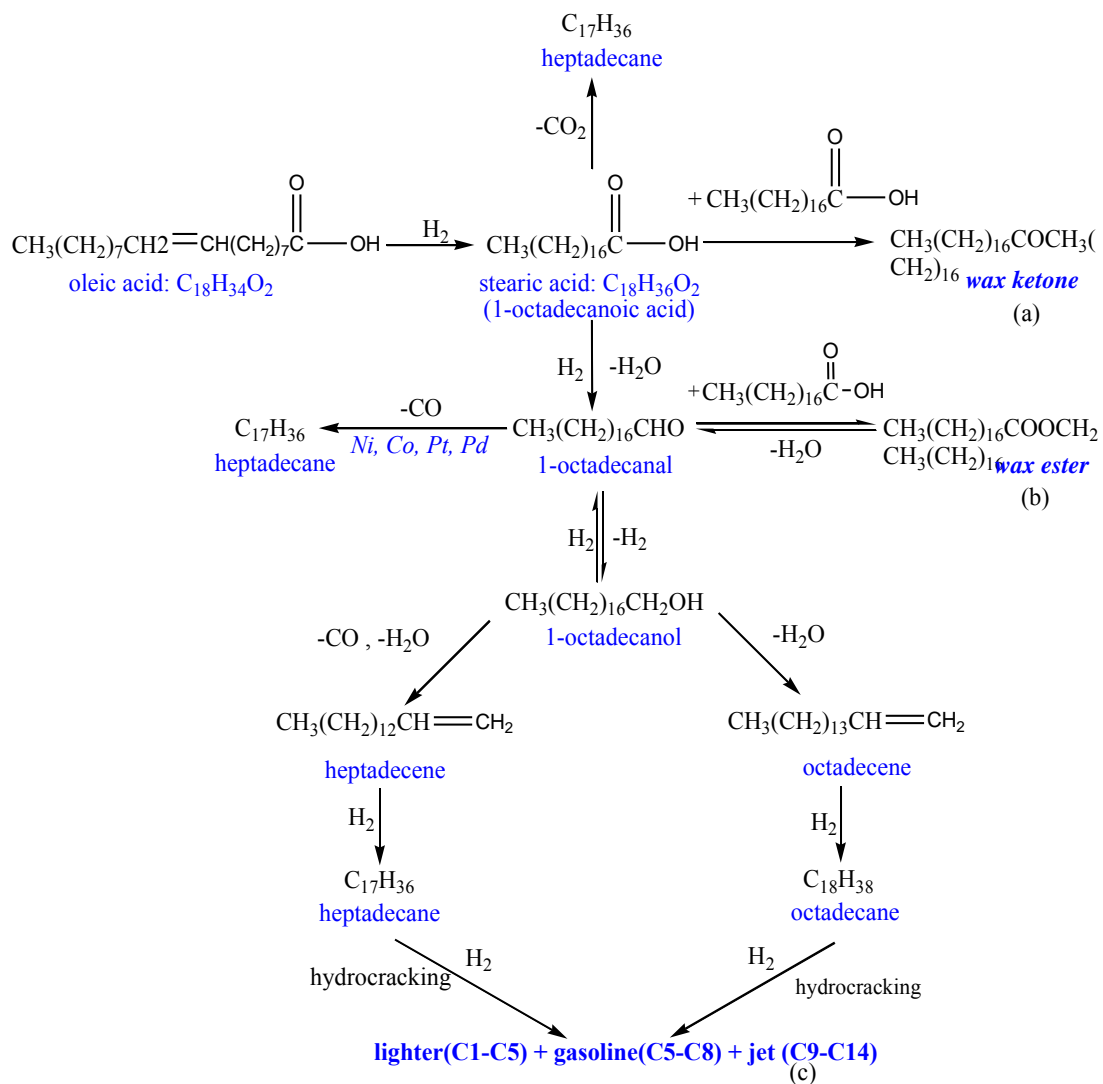


Figure 4.32 Proposed reaction pathways of oleic acid to hydrocarbons.

4.5 Characterization of Spent Catalysts

4.5.1 Temperature-Programmed Oxidation (TPO)

Figure 4.33 and Table 4.4 illustrate the TPO profiles and amounts of coke deposit of spent catalysts after 8 h on stream, respectively. The Pd/TiO₂ catalyst exhibited the lowest coke formation at 8.3 wt. % while the Ni/HY catalyst exhibited the highest coke formation at 22.8 wt. % because Brønsted acid sites were selective for catalyst cracking process. The peaks observed at temperatures below 450 °C represented the weakly coke deposit on the support. The Ni/HY^{core}-Pd/TiO₂^{shell} catalyst showed combined patterns of parent catalyst and comparable amount of coke contained lower oxidation temperature than Ni/HY parent catalysts. It was because the deoxygenation produced fatty alcohol as an intermediates which could be further diffused into the pore of zeolite if the coke was formed, while the acid sites Ni/HY parent catalyst was poisoning by the role of water from hydrodeoxygenation of feed or pore blockage by large molecules lead to higher hard coke formation.

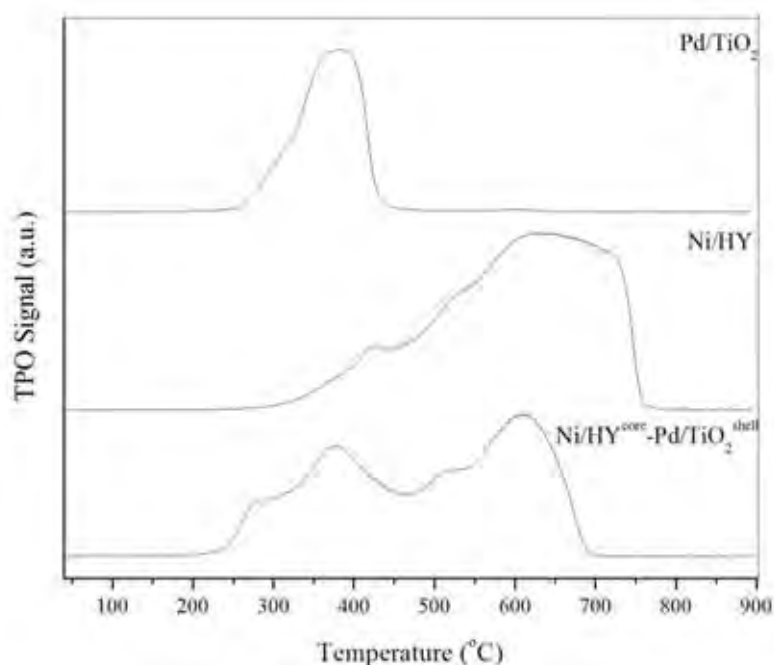


Figure 4.33 TPO profiles of Ni/HY^{core}-Pd/TiO₂^{shell}, Ni/HY, and Pd/TiO₂ catalysts after 8 h course of reaction.

Table 4.4 Amount of carbon deposits on prepared catalyst after reaction

Spent Catalysts	Coke (wt. %)
Ni/HY^{core}-Pd/TiO₂^{shell}	17.4
Ni/HY	22.8
Pd/TiO₂	8.3

CHAPTER V

CONCLUSIONS AND RECOMMENDATIONS

5.1 Conclusions

The synthesized Ni/HY^{core}-Pd/TiO₂^{shell} catalyst can be confirmed the containing parent catalyst structures by XRD results and TEM images. TEM images revealed the coverage of shell layer which on core catalyst. The characteristic of a mesoporous structure in TiO₂ provided the decreasing of BET surface area and pore volume of Pt/HY^{core}-Pd/TiO₂^{shell} catalysts. The Ni/HY^{core}-Pd/TiO₂^{shell} catalysts exhibited 100 % conversion of PFAD and gaves highest selectivity (48%) toward to bio-jet fuel at reaction condition 425 °C, 30 bar, H₂/feed molar ratio 10, and LHSV 1.5 h⁻¹. Therefore, the effect of lowering temperature gives high diesel hydrocarbon production while increasing temperature up to 450 °c exhibited high cracking reaction and produce more lighter gas thus the appropriate temperature was 425 °C. In addition, the effect of increasing pressure was influenced higher selective bio-jet fuels production due to an intermediate is more converted to bio-jet fuel. The formation of hydrocarbons from fatty acid over core-shell catalyst occurs through an aldehyde and alcohol intermediates further transform to heavier hydrocarbon then subsequently hydrocracking/hydroisomerization to bio-jet fuel.

5.2 Recommendations

In this work, the synthesized catalyst exhibited 100 % conversion for 8 h of the reaction and seem to be stable until 8 h. Nonetheless, the selectivity towards to diesel slightly increase with time related to the selectivity towards to bio-jet fuel gradually dropped down thus it could be possible that that the core catalyst might be deactivated with the more time on stream. For this reason, the core catalyst should be further studied.

In order to improve biojet fuel production from PFAD, ketonization reaction can be occurred with the TiO_2 and incorporate between feed and intermediates lead to large molecules can be also occurred thus those all preliminary problems should be inhibited by inert support so the catalyst has to develop further in the future work to gain more bio-jet fuel production.

REFERENCES

- Amin T.K. and Hossein M., (2013) Processes of biodiesel production from waste cooking oil. Applied Energy, 104, 683-710.
- Borghet, K.V.D. (2009) Experimental study and kinetic modeling of the synergy in hydro-isomerisation under industrial conditions. M.S. Thesis, University of Ghent, Ghent, Belgium.
- Bovornseripatai, P., Jongpatiwut, S., Osuwan, S., and Butnark, S. (2012) Effect of biomass feedstocks on the production of hydrogenated biodiesel. World Academy of Science, Engineering and Technology International Journal of Chemical, Molecular, Nuclear, Materials and Metallurgical Engineering, 6(4), 265-269.
- Busca, G. (2014) Heterogeneous Catalytic Materials. The Netherlands: Elsevier.
- Bartholomew, C., and Farrauto, R. (2005) Fundamentals of Industrial Catalytic Processes, New Jersey: John Wiley & Sons.
- Cheng, J., Li, T., Huang, R., Zhou, J., and Cen, K (2014) Optimizing catalysis conditions to decrease aromatic hydrocarbons and increase alkanes for improving jet biofuel quality. Bioresource Technology, 158, 378-382.
- De Lucas, A., Sánchez, P., Fúnez, A., Ramos, M., and Valverde, J. (2006) Influence of clay binder on the liquid phase hydroisomerization of *n*-octane over palladium-containing zeolite catalysts. Journal of Molecular Catalysis A: Chemical, 259(1), 259-266.
- Deldari, H. (2005) Suitable catalysts for hydroisomerization of long-chain normal paraffins. Applied Catalysis A: General, 293, 1-10.
- Dupont, C., Lemeur, R., Daudin, A., and Raybaud, P. (2011) Hydrodeoxygenation pathways catalyzed by MoS₂ and NiMoS active phases: A DFT study. Journal of Catalysis, 279, 276-286.
- Hagen, J. (1999) Industrial Catalysis: A Practical Approach. Wiley-VCH: Weinheim.

- Dhanapalan Karthikeyan, D., Atchudan, R., and Sivakumar, R. (2016) Effect of metal content on the activity and product selectivity of *n*-decane hydroisomerization over Ni-Pd/HY zeolite. Chinese Journal of Catalysis, 37, 1907-1917.
- Kordulisa, C., Bourikas, K., Gousi, M., Kordouli, E., and Lycourghiotis, A. (2016) Development of nickel based catalysts for the transformation of natural triglycerides and related compounds into green diesel: a critical review. Applied Catalysis B: Environmental, 181, 156-196.
- Lee, H.W., Jeon, J.-K., Jeong, K.-E., Kim, C.-U., Jeong, S.-Y., Han, J., and Park, Y.-K. (2013) Hydroisomerization of *n*-dodecane over Pt/Y zeolites with different acid characteristics. Chemical Engineering Journal, 232, 111-117.
- Li, J., Tian, W., and Shi, L. (2010) Hydrogenation of maleic anhydride to succinic anhydride over Ni/HY-Al₂O₃. Industrial and Engineering Chemistry Research, 49(22), 11837-11840.
- Nishimura, S. (2001) Handbook of Heterogeneous Catalytic Hydrogenation for Organic Synthesis. United States of America: John Wiley & Sons.
- Okada, S., Ikurumi, S., Kamegawa, T., Mori, K., and Yamashita, H. (2012) Structural design of Pd/SiO₂@ Ti-containing mesoporous silica core-shell catalyst for efficient one-pot oxidation using in situ produced H₂O₂. The Journal of Physical Chemistry C, 116(27), 14360-14367.
- Onga, H.C., Mahlia, T.M.I., Masjukia, H.H., and Norhasyimab, R.S. (2011) Comparison of palm oil, *Jatropha curcas* and *Calophyllum inophyllum* for biodiesel: a review. Renewable and Sustainable Energy Reviews, 15, 3501-3515.
- Peng, B., Yao, Y., Zhao, C., and Lercher, J. A. (2011) Towards quantitative conversion of microalgae oil to diesel-range alkanes with bifunctional catalysts. Angewandte Chemie International Edition, 51, 2072-2075.
- Santos, R.C.R., Valentini, A., Lima, C.L., Josue Filho, M., and Oliveira, A.C. (2011) Modifications of an HY zeolite for *n*-octane hydroconversion. Applied Catalysis A: General, 403(1), 65-74.

- Scherzer, J. and Gruia, A.J. (1996) Hydrocracking Science and Technology. United States of America: Marcel Dekker.
- Shen, S., Garces, L., Ding, Y., Laubernds, K., Zerger, R., Aindow, M., Neth, E., and Suib, S. (2008) Behavior of H₂ chemisorption on Ru/TiO₂ surface and its application in evaluation of Ru particle sizes compared with TEM and XRD analyses. Applied Catalysis A: General, 335, 187-195.
- Siregar, K., Tambunan, A.H., Irwanto, A.K., Wirawan, S.S., and Araki, T. (2015) A comparison of life cycle assessment on oil palm (*Elaeis guineensis* Jacq.) and physic nut (*Jatropha curcas* Linn.) as feedstock for biodiesel production in Indonesia. Energy Procedia, 65, 170-179.
- Sooknoi, T. (1994) Zeolites and Related Microporous Materials. The Netherlands: Elsevier.
- Suzuki, M., Tsutsumi, K., Takahashi, H., and Saito, Y. (1989) T.P.R. study on reducibility of nickel ions in zeolite Y. Zeolites, 9, 98-103.
- Talebian-Kiakalaieh, A., Amin, N. A. S., and Hossein, M. (2013) A review on novel processes of biodiesel production from waste cooking oil. Applied Energy, 104, 683-710
- Tamiyakul, S., Anutamjarikun, S., and Jongpatiwut, S. (2016) The effect of Ga and Zn over HZSM-5 on the transformation of palm fatty acid distillate (PFAD) to aromatics. Catalysis Communications, 74, 49-54.
- Wan, Z. and Hameed, B.H. (2014) Chromium–tungsten–titanium mixed oxides solid catalyst for fatty acid methyl ester synthesis from palm fatty acid distillate. Energy Conversion and Management, 88, 669-676.

APPENDIX

Appendix A Overall Mass Balance of Deoxygenation-hydroprocessing at Different in Temperature (375, 400, 425, 450 °C)

Table A1 Overall mass balance of deoxygenation-hydroprocessing one-pot reaction over 5%Ni/HY^{core}-1%Pd/TiO₂^{shell} catalyst at different in temperature. (Reaction condition: 5 bar, H₂/feed molar ratio of 10, LHSV of 1.5 h⁻¹, and TOS at 6h)

Temperature (°C)		375 °C	400 °C	425 °C	450 °C
Selectivity of gas product (wt. %)	C1	7.428369	6.644078	1.725199	15.552
	C2	0.544218	0.594578	0.21771	2.18578
	C3	3.101488	2.378224	0.197376	4.689122
	C4	10.14418	5.707234	1.657015	8.994222
	iso-C5	0	0	0	0
	C5	1.739575	0.907166	0.185992	1.24353
	iso-C6	5.583653	4.01719	1.052989	5.01771
	C6	0.969745	0.634647	0.088259	0.635332
	iso-C7	1.993175	2.755547	0.620938	2.836679
	C7	2.101681	0.95458	0.118233	0.829018
	iso-C8	0	0	0	0
	C8	0	0	0	0
	iso-C9	0	0	0	0
	C9	0	0	0	0

Table A1 (Cont.) Overall mass balance of deoxygenation-hydroprocessing one-pot reaction over 5%Ni/HY^{core}-1%Pd/TiO₂^{shell} catalyst at different in temperature. (Reaction condition: 5 bar, H₂/feed molar ratio of 10, LHSV of 1.5 h⁻¹, and TOS at 6h)

Temperature (°C)		375 °C	400 °C	425 °C	450 °C
Selectivity of liquid product (wt. %)	iso-C7	0	0	0	0
	n-C7	0.498571	0	0	0.305942
	iso-C8	0	0	59.01952	0
	n-C8	0	0.098477	132.0297	0.393419
	iso-C9	1.973079	1.093707	409.7327	3.268882
	n-C9	0.577601	0.881014	391.6746	0.855038
	iso-C10	2.237738	2.668096	4.334837	3.106427
	n-C10	0.445368	0.51088	1.138272	1.079038
	iso-C11	1.310877	3.306406	6.124837	4.400205
	n-C11	0.539435	0.595249	0.795149	0.720666
	iso-C12	1.326645	3.872918	7.336712	4.547207
	n-C12	0.5126	0.74439	0.480131	0.720666
	iso-C13	1.333638	4.196901	5.54198	3.806219
	n-C13	1.025057	1.578667	1.983421	0.694738
	iso-C14	1.077663	4.079305	5.401613	4.489472
	n-C14	1.311977	0.74439	2.948686	1.788083
	iso-C15	3.909458	4.959043	5.700533	3.70343
	n-C15	10.9486	7.868254	8.103172	6.026111
	iso-C16	4.646742	5.33295	9.052584	3.806354
	n-C16	3.326782	2.039541	0.662157	0.924587
iso-C17	4.143457	5.278248	5.561957	3.666485	
n-C17	8.081251	3.16028	2.713927	1.47771	
iso-C18	1.522316	3.751087	5.850517	3.06436	
n-C18	1.946853	0.755136	0.378195	0.390679	
Feed Remaining		34.39944	0.282293	0.92416	0.52425
Intermediates		13.69821	17.89182	17.01675	4.780888
% Conversion		74.40507	99.7185	99.0843	99.47848

Appendix A Overall Mass Balance of Deoxygenation-hydroprocessing at Different in Pressure (5, 10, 15, 30 bar)

Table A2 Overall mass balance of deoxygenation-hydroprocessing one-pot reaction over 5%Ni/HY^{core}-1%Pd/TiO₂^{shell} catalyst at different in pressure. (Reaction condition: 425 °C, H₂/feed molar ratio of 10, LHSV of 1.5 h⁻¹, and TOS at 6h)

Pressure (bar)		5	10	15	30
Selectivity of gas product (wt. %)	C1	1.725199	7.213124	4.914664	0.862827
	C2	0.21771	0.953443	0.758254	0.21512
	C3	0.197376	3.959884	3.186118	1.094761
	C4	1.657015	12.32447	7.258534	2.378053
	iso-C5	0	0	0	0
	C5	0.185992	2.298069	0.828276	0.152837
	iso-C6	1.052989	7.757662	2.357658	0.060465
	C6	0.088259	1.798518	0.38778	0.013933
	iso-C7	0.620938	3.514882	0.342882	0
	C7	0.118233	0.355978	0	0
	iso-C8	0	0	0	0
	C8	0	0	0	0
	iso-C9	0	0	0	0
	C9	0	0	0	0

Table A2 (Cont.) Overall mass balance of deoxygenation-hydroprocessing one-pot reaction over 5%Ni/HY^{core}-1%Pd/TiO₂^{shell} catalyst at different in pressure. (Reaction condition: 425 °C, H₂/feed molar ratio of 10, LHSV of 1.5 h⁻¹, and TOS at 6h)

Pressure (bar)		5	10	15	30
Selectivity of liquid product (wt. %)	iso-C7	0	0	0	0
	n-C7	0	2.509009995	3.94019096	2.761517741
	iso-C8	59.01952171	0.289485559	0.581237831	0.818906708
	n-C8	132.0296783	0.58164231	1.115073671	1.633526803
	iso-C9	409.7326908	0.659696758	1.099646475	2.091926352
	n-C9	391.6745911	1.085454003	1.945367711	3.06025674
	iso-C10	4.334836866	3.22995079	5.850615691	9.629751425
	n-C10	1.138271746	0.9038078	1.709745037	3.452076212
	iso-C11	6.124836693	4.155551797	5.368788504	9.466123377
	n-C11	0.795149074	0.662182403	1.348134271	1.882895128
	iso-C12	7.336712375	3.740908149	4.182271682	6.809245297
	n-C12	0.480131272	0.880926607	1.605351019	2.228907847
	iso-C13	5.541980222	3.7902158	3.505538832	5.257445167
	n-C13	1.983421287	1.523004567	2.513585228	1.446042576
	iso-C14	5.401613157	2.793132797	2.113823416	6.686686491
	n-C14	2.948686267	2.114139497	3.730367764	5.199092756
	iso-C15	5.700533418	3.18155694	2.767918982	3.969224025
	n-C15	8.103172407	6.97439881	12.94832025	13.7209561
	iso-C16	9.052583578	3.892875747	3.500163503	4.077902939
	n-C16	0.662156902	1.587146922	2.633424417	2.847635425
iso-C17	5.56195738	3.773007902	3.743310734	1.583339419	
n-C17	2.713926677	2.250065496	3.972901036	3.607254808	
iso-C18	5.850517168	3.076856675	2.08516742	1.033852124	
n-C18	0.378194902	0.586144551	0.79959213	0.814557803	
Feed Remaining		0.92416	0.591567	0.20422	0
Intermediates		17.01675	5.582812	6.905297	1.142881
% Conversion		99.0843	99.41191	99.7962	100

Appendix A Overall Mass Balance of Deoxygenation-hydroprocessing at Different in Liquid Hourly Space Velocity (1.5, 2.0, 2.5 h⁻¹)

Table A3 Overall mass balance of deoxygenation-hydroprocessing one-pot reaction over 5%Ni/HY^{core}-1%Pd/TiO₂^{shell} catalyst at different in LHSV. (Reaction condition: 425 °C, pressure 30 bar, H₂/feed molar ratio of 10, and TOS at 6h)

LHSV (h ⁻¹)		1.5	2	2.5
Selectivity of gas product (wt. %)	C1	0.862826629	1.069211421	4.192117778
	C2	0.21511991	0.090374727	0.742540123
	C3	1.094761101	0.902896337	2.915455038
	C4	2.378052548	3.651539506	5.598170061
	iso-C5	0	0	0
	C5	0.152837177	0.470152457	0.698184619
	iso-C6	0.060465334	1.065873732	1.29961263
	C6	0.013932894	0.244123319	0.287816339
	iso-C7	0	0.158820638	0.24020294
	C7	0	0.540942074	0.000478449
	iso-C8	0	0	0
	C8	0	0	0
	iso-C9	0	0	0
	C9	0	0	0

Table A3 (Cont.) Overall mass balance of deoxygenation-hydroprocessing one-pot reaction over 5%Ni/HY^{core}-1%Pd/TiO₂^{shell} catalyst at different in LHSV. (Reaction condition: 425 °C, pressure 30 bar, H₂/feed molar ratio of 10, and TOS at 6h)

LHSV (h ⁻¹)		1.5	2	2.5
Selectivity of liquid product (wt. %)	iso-C7	0	0	0
	n-C7	2.761517741	0.75271612	0.267208757
	iso-C8	0.818906708	2.05330964	0.088396955
	n-C8	1.633526803	1.073148501	0.655169723
	iso-C9	2.091926352	0.100624233	0.718405511
	n-C9	3.06025674	0.65905218	1.713667288
	iso-C10	9.629751425	2.486955834	3.250326312
	n-C10	3.452076212	0.210072781	0.964702466
	iso-C11	9.466123377	2.119349374	4.026544292
	n-C11	1.882895128	0.505151426	0.314931176
	iso-C12	6.809245297	1.165046288	3.652487104
	n-C12	2.228907847	0.616359402	1.243088473
	iso-C13	5.257445167	0.334536999	4.370098217
	n-C13	1.446042576	0.6351482	1.935470026
	iso-C14	6.686686491	0	3.775887953
	n-C14	5.199092756	1.07641035	2.709875145
	iso-C15	3.969224025	2.100255031	4.562644579
	n-C15	13.7209561	13.91428113	10.10609539
	iso-C16	4.077902939	6.087301319	4.912947963
	n-C16	2.847635425	16.54979979	2.012875452
iso-C17	1.583339419	4.210181529	6.095820543	
n-C17	3.607254808	11.50609001	3.490286228	
iso-C18	1.033852124	4.046396228	3.98543321	
n-C18	0.814557803	10.79388037	1.058248394	
Feed Remaining		0	7.07744942	16.05876495
Intermediates		1.142881139	8.809999051	18.11481086
% Conversion		99.0843021	93.39034553	86.16324673

Appendix A Overall Mass Balance of Deoxygenation-hydroprocessing One-pot Reaction over Pd/TiO₂, Ni/HY, and 5%Ni/HY^{core}-1%Pd/TiO₂^{shell} Catalysts

Table A4 Overall mass balance of deoxygenation-hydroprocessing one-pot reaction over Pd/TiO₂, Ni/HY, and 5%Ni/HY^{core}-1%Pd/TiO₂^{shell} catalysts. (Reaction condition: 425 °C, pressure 30 bar, H₂/feed molar ratio of 10, LHSV of 1.5 h⁻¹ and TOS at 6h)

Catalyst		Pd/TiO ₂ (shell)	Ni/HY (core)	Ni/HY ^{core} - Pd/TiO ₂ ^{shell}
Selectivity of gas product (wt. %)	C1	5.381690002	2.184124446	0.862826629
	C2	0.729288032	0.38116312	0.21511991
	C3	1.374072844	2.075202933	1.094761101
	C4	1.552101108	9.243347915	2.378052548
	iso-C5	0	0	0
	C5	0.05588917	1.33757722	0.152837177
	iso-C6	0.108896006	1.71181012	0.060465334
	C6	0.772676563	0.393859513	0.013932894
	iso-C7	0	0	0
	C7	0.489410424	0	0
	iso-C8	0	0	0
	C8	0	0	0
	iso-C9	0	0	0
	C9	0	0	0

Table A4 (Cont.) Overall mass balance of deoxygenation-hydroprocessing one-pot reaction over 5%Ni/HY^{core}-1%Pd/TiO₂^{shell} catalyst at different in LHSV. (Reaction condition: 425 °C, pressure 30 bar, H₂/feed molar ratio of 10, LHSV of 1.5 h⁻¹ and TOS at 6h)

Catalyst		Pd/TiO ₂ (shell)	Ni/HY (core)	Ni/HY ^{core} - Pd/TiO ₂ ^{shell}
Selectivity of liquid product (wt. %)	iso-C7	0	0	0
	n-C7	0	1.007510774	2.761517741
	iso-C8	0.297713688	0.648934142	0.818906708
	n-C8	0.232425381	16.76921936	1.633526803
	iso-C9	0.391219851	0.740278245	2.091926352
	n-C9	2.686995723	1.804308851	3.06025674
	iso-C10	0.947436219	3.018376685	9.629751425
	n-C10	2.49926563	0.975722691	3.452076212
	iso-C11	0.290588364	5.158289208	9.466123377
	n-C11	2.911186253	0.279710907	1.882895128
	iso-C12	0.389594165	3.644292307	6.809245297
	n-C12	2.75390044	0.90263108	2.228907847
	iso-C13	0.451773001	3.912076988	5.257445167
	n-C13	3.875556396	1.437172863	1.446042576
	iso-C14	0.428307092	2.730561085	6.686686491
	n-C14	5.925769527	2.049915793	5.199092756
	iso-C15	1.095718753	4.080457596	3.969224025
	n-C15	8.281376077	15.86040085	13.7209561
	iso-C16	1.364812791	3.53964445	4.077902939
	n-C16	6.052149428	1.471034384	2.847635425
iso-C17	1.282929836	3.148531278	1.583339419	
n-C17	7.633740488	3.048760283	3.607254808	
iso-C18	1.073393298	2.111432365	1.033852124	
n-C18	2.835458648	0.394405542	0.814557803	
Feed Remaining		2.183344429	1.693505176	0
Intermediates		35.8346648	3.939247	1.142881139
% Conversion		97.86330694	98.33469682	100

